Title: Ca^{2+}-driven nanodomain enrichment and plasma membrane proteome remodelling enable bacterial outer membrane vesicle perception in rice

Authors: Ishani Mondal[1], Hrimeeka Das[1,2], Smrutisanjita Behera*[1,2].

Author Affiliations:

[1] Infectious Diseases and Immunology Division, CSIR-Indian Institute of Chemical Biology, 4, Raja S. C. Mullick Road, Kolkata-700032, India.

[2] Academy of Scientific and Innovative Research (AcSIR), Ghaziabad, India

*For correspondence (email: smrutisanjita@gmail.com, sbehera.iicb@csir.res.in)

Sections:

- **Summary:** 165 words
- **Introduction:** 773 words
- **Materials and Methods:** 1924 words
- **Results:** 2503 words
- **Discussion:** 1295 words

Total word count: 6882 words (Including Summary)

Figures: 6 main figures (should be in colour)

Tables: 2 main tables.

Supporting information:

- 4 Supporting figures.
- 2 Supporting tables.
- 1 Supporting video.

Ca^{2+}-driven nanodomain enrichment and plasma membrane proteome remodelling enable bacterial outer membrane vesicle perception in rice

Ishani Mondal[1], Hrimeeka Das[1,2], Smrutisanjita Behera*[1,2].

[1] Infectious Diseases and Immunology Division, CSIR-Indian Institute of Chemical Biology, 4, Raja S. C. Mullick Road, Kolkata-700032, India.

[2] Academy of Scientific and Innovative Research (AcSIR), Ghaziabad, India

*For correspondence (email: smrutisanjita@gmail.com, sbehera.iicb@csir.res.in)

Summary:

1. *Xanthomonas oryzae pv. oryzae* (*Xoo*) releases OMVs; however, the role of *Xoo*-OMVs in *Xoo*-rice interaction has not yet been studied. We investigated the early signalling events underlying *Xoo*-OMV perception by rice to gain insight into early plant-pathogen interactions.
2. We observed that *Xoo*-OMVs are perceived by rice through a rapid and unique Ca^{2+} signal that is essential to evoke an immune response. By confocal imaging and proteomic analysis of the rice PM, we found that the Ca^{2+} signal is required for *Xoo*-OMV-induced nanodomain enrichment and for the aggregation of defence response-associated proteins in rice PM.
3. The differential assembly of proteins in the PM helps the plant defend itself against *Xoo*. In the absence of the early Ca^{2+} signal, *Xoo*-OMVs are not perceived by the plant, resulting in a compromised immune response.
4. Collectively, our study shows that *Xoo*-OMVs are recognised by rice via Ca^{2+} signal-induced nanodomain assembly leading to protein reorganisation in the PM to prepare the plant for an imminent pathogen invasion.

Keywords:

Calcium signalling, Nanodomain, *Oryza sativa* (Rice), Outer membrane vesicles (OMVs), Plant-pathogen interaction, Plasma membrane, *Xanthomonas oryzae pv. oryzae* (*Xoo*).

Introduction

Xanthomonas oryzae pv. oryzae (*Xoo*) is a gram-negative bacterium that causes Bacterial Blight of rice (Oryza sativa), leading to a significant loss of rice yield (Niño-Liu et al., 2006). To protect rice against *Xoo*, more than 45 resistant (R) genes have been identified, which are expressed in susceptible varieties through breeding or transgenic approaches to confer resistance against *Xoo*. However, majorly cultivated rice varieties still remain susceptible as it is extremely difficult and tedious to replace hundreds of cultivated varieties by transgenic or gene-edited varieties. To provide sustainable resistance against *Xoo*, a basic understanding of early *Xoo*-rice interaction is necessary. In this context, we explored the inter-kingdom communication between rice and *Xoo* through *Xoo*-released Outer Membrane Vesicles (OMVs). OMVs are spherical nano-proteo-liposomal vesicles released by Gram-negative bacteria to carry out functions like biofilm formation, quorum sensing, virulence, communication, etc., thereby helping the bacteria to adapt to its surroundings (Kulp and Kuehn, 2010; McBroom and Kuehn, 2007; Sartorio et al., 2021).

The role of bacterial OMVs in plant-pathogen interaction is not as extensively explored as it has been in animal-pathogen interaction. Isolation and proteomic characterisation of OMVs from phytopathogenic bacteria, like *Xylella fastidiosa, Xanthomonas campestris pv. campestris* (*Xcc*), *Pseudomonas syringae pv. tomato (Pst)*, *Pectobacterium brasiliense,* and *Candidatus liberibacter* (Chowdhury and Jagannadham, 2013; Huang et al., 2022; Maphosa and Moleleki, 2021; Mendes et al., 2016; Sidhu et al., 2008) have identified several OMV-associated proteins, like outer membrane proteins (OMPs), and virulence factors, including T3SS secretion proteins, cell wall-degrading enzymes, porins, lipases, etc. (Chowdhury and Jagannadham, 2013; Jang et al., 2014; Sidhu et al., 2008). OMVs produced by *Xcc* carry MAMPs, such as flg22, EF-Tu, etc. and elicit a PRR-mediated immune response in Arabidopsis (Bahar et al., 2016; Feitosa-Junior et al., 2019; Chalupowicz et al., 2023). *Xcc*-OMVs potentiate nanodomain enrichment, leading to insertion of *Xcc*-OMVs into the host plasma membrane (PM), which further increases the membrane order and reinforces a positive feedback loop to amplify immune responses against the pathogen (Tran et al., 2022). Nanodomains are nanoscale proteo-lipid congregations in the PM that mediate plant responses to biotic and abiotic stress (Gronnier et al., 2017; Jaillais and Ott, 2020; Nagano et al., 2016). For example, specialised nanodomain aggregation is crucial for defining the spatiotemporal specificity of the FLS2 and BRI1-

mediated immune pathways in Arabidopsis (Ott, 2017; Bücherl et al., 2017). However, what drives such signal-specific nanodomain enrichment remained unknown.

Parallel to nanodomain enrichment, Ca^{2+} signalling is another indispensable early event for a plant's immune response. For example, sustained Ca^{2+} increase is observed during the HR response in Arabidopsis challenged by *Pseudomonas syringae* (Grant et al., 2000). Ca^{2+} permeable channels like CNGC2 and CNGC4 are important in shaping PTI-induced Ca^{2+} signals (Ali et al., 2007; Tian et al., 2019). MAMPs like flg22, chitin, elf 18, and pep1, can induce stimulus-specific Ca^{2+} signatures in Arabidopsis mediated by RLCKs, PBL1, and BIK1 (Cao et al., 2017; Keinath et al., 2015; Ranf et al., 2014, 2015). Interestingly, CPK3 can phosphorylate the intrinsically disordered domain (IDD) of REM1.3, a PM nanodomain-associated protein, and thereby influence the function of REM1.3 during plant-virus interaction (Perraki et al., 2018), indicating the role of Ca^{2+}-binding proteins in nanodomain clustering. These findings prompted us to investigate the involvement of Ca^{2+} signals in nanodomain aggregation and signal transduction during perception of OMVs by plants.

In this work, we have explored the early events during *Xoo*-rice interaction. We have isolated OMVs from *Xoo,* identified the *Xoo*-OMV-associated proteins and examined how rice (*Oryza sativa subsp. indica*) responds to *Xoo*-OMVs. To this end, we have used one susceptible variety of rice, Khitish, and a resistant variety of rice, CR 800. CR 800 expresses three R genes- *xa13*, *xa5,* and *Xa21,* that render it resistant to *Xoo* infection (Mohapatra et al., 2023). Through proteomic analysis, we have found that *Xoo*-OMVs carry abundant MAMPs like EF-Tu, flagellin, Ax21, etc. and elicit a rapid and unique Ca^{2+} signal in the roots of both host rice and non-host Arabidopsis. We have further witnessed that *Xoo*-OMVs can rapidly increase the lipid order of the rice PM and facilitate sterol-mediated insertion of the *Xoo*-OMVs into the PM. We have found that both the above events are Ca^{2+}-dependent. Furthermore, the immune response of CR 800 against the *Xoo*-OMVs is diminished in Ca^{2+}-deprived condition. Quantitative proteomic analysis of the *Xoo*-OMV-treated CR 800 PM revealed that *Xoo*-OMVs increase the abundance of defence response-related proteins in the PM in the presence of Ca^{2+} but not in a Ca^{2+}-chelated condition. Collectively, our results describe the Ca^{2+}-dependent relay of events during the perception of OMVs by the host plant and contribute to the understanding of early host-pathogen interaction.

Materials and Methods:

Plant and bacterial samples:

Khitish (susceptible to *Xoo,* does not have R genes) and CR 800 (resistant to *Xoo*, contains R genes, Xa21, xa3, xa15) (*Oryza sativa subsp. indica*) were grown hydroponically at 30 ºC under a 14-hour light / 10-hour dark condition, with 70-80% humidity. Col-0-RGECO1 (Col-0 plants expressing the genetically encoded Ca^{2+} indicator (GECI), RGECO1 were grown in 0.5 strength MS media at 22 ºC. *Xanthomonas oryzae pv. oryzae* strain BXO43 (rifampicin derivative of BXO1, a Bengal isolate, (Rajagopal et al., 1997) was grown in peptone sucrose (PS) media ($O.D._{600}$ of 0.6) with rifampicin (50 µg/ml) at 28 ºC.

Isolation of outer membrane vesicles:

Xoo-OMVs were isolated and purified according to the protocol of Mordukhovich and Bahar, 2017. Briefly, the supernatant of the BXO43 culture was filtered through a 0.45 µm syringe filter to obtain the cell-free supernatant. It was ultracentrifuged at a speed of 100000g at 4 ºC for 2 hours and filtered again through a 0.22 µm filter followed by another wash to remove contaminant proteins. This crude *Xoo*-OMV preparation was loaded on top of a density gradient of 45%, 40%, 35%, 30%, 25%, and 20% of OptiPrep diluent buffer (Sigma) for purification. Each fraction was collected and washed twice to remove the diluent buffer. The resultant purified *Xoo*-OMV pellet was weighed and re-suspended in sterile deionized water or in Ca^{2+} imaging buffer as per the requirement of the experiment, at a concentration of 100 mg/ml fresh weight. Isolated *Xoo*-OMVs were stored at 4 ºC and utilized within 3 days of isolation. The total protein content of the *Xoo*-OMVs was quantified using Bradford assay (Biorad).

Nanoparticle Tracking Analysis (NTA):

The *Xoo*-OMVs were diluted 200 times in sterile water and injected into the laser chamber of Nanosight NS300. The videos were analysed and plotted in a graph using the NTA 3.2 Dev Build 3.2.16 software.

Atomic force microscopy (AFM):

Xoo cells were diluted with PBS to an O.D. of 0.2. The diluted *Xoo* cells were incubated at 28 ºC for 1 hour. 3 µl of the cells were dropped on a freshly cleaved mica sheet. The sheet was

122 dried inside a vacuum desiccator for 1 hour and visualized with the help of the AFM-MFP-3D
123 (Oxford Instruments) in tapping mode.

124 **Transmission electron microscopy (TEM):**

125 *Xoo*-OMVs were fixed in 2% glutaraldehyde, and 5 µl of the sample was dropped on a copper
126 grid. The sample was stained with 1% uranyl acetate and visualized under a Jeol-JEM-2100
127 Plus transmission electron microscope.

128 **Isolation of PM-associated proteins from CR 800:**

129 7-day-old CR 800 seedlings were incubated for 1 hour in sterile water (Control) or in *Xoo*-
130 OMVs (OMV). For Ca^{2+}-chelation, seedlings were treated with 2 mM EGTA for 30 minutes
131 before incubation in *Xoo*-OMVs (EGTA-OMV) for 1 hour. PM was isolated from the roots
132 according to the protocol described in (Uemura et al., 1995). Briefly, roots of ~ 4000 seedlings
133 were homogenised in homogenising buffer (0.5 M sorbitol, 50 mM Mops-KOH (pH 7.6), 5
134 mM EGTA (pH 8.0), 5 mM EDTA (pH 8.0), 5% (w/v) PVP-40, 0.5% (w/v) BSA, 2.5 mM
135 PMSF,4 mM SHAM, 2.5 mM DTT). The homogenate was centrifuged to remove debris and
136 ultracentrifuged to obtain the microsomal fraction. The microsomal fraction was enriched with
137 PM proteins by a repeated two-phase partitioning system using PEG-dextran (6%, w/w). The
138 enriched PM proteins were washed twice and re-suspended in PM suspension buffer (10 mM
139 Mops-KOH (pH 7.3), 2 mM EGTA (pH 8.0), 0.25 M sucrose) for further proteomic analysis.
140 Three such independent biological replicates were performed for each sample (Control, EGTA-
141 OMV, OMV).

142 **SDS-PAGE and in-gel trypsin digestion:**

143 Proteins were precipitated from the *Xoo*-OMV samples using water: methanol:
144 chloroform=4:3:1. The protein pellet was recovered from the interface of the aqueous and
145 organic phases, washed with methanol and dried. CR 800-PM proteins and *Xoo*-OMV proteins
146 were resuspended in 1X Tris-glycine sample loading buffer (Invitrogen). 50 µg of each
147 replicate of the respective protein samples were run separately in a 12% SDS-PAGE gel. After
148 brief staining with Coomassie blue G-250 the protein bands were cut, de-stained with
149 ammonium bicarbonate and dehydrated with ACN. The proteins were digested with trypsin for
150 15 minutes, followed by protein extraction for 24 hours. An additional step of 1 hour of protein

151 extraction was carried out in order to maximize the peptide concentration. The peptides were
152 lyophilized and stored at -20 ºC until further analysis through the ESI-MS/MS system.

153 **LC-ESI-MS/MS of digested peptides:**

154 The digested peptides (of both *Xoo*-OMV proteins and CR 800-PM proteins) were
155 reconstituted in 10 µl of 1% formic acid and 0.75 µg of peptides were subjected to the nano-
156 flow (75 µm x 500 mm, EASY-Spray™ PepMap™ Neo C18 column, with 100 Å pore size) of
157 an Orbitrap Fusion Lumos mass spectrometer (Thermo Fisher Scientific). The system was run
158 for 140 minutes with Solvent A=0.1% formic acid and Solvent B=80% ACN 0.1% formic acid.
159 The peptides were eluted at a constant flow of 0.3 µl/min, starting with 5% solvent B to 75%
160 solvent B up to 125 minutes, then decreasing to 5% solvent B until 140 minutes. The scan was
161 performed in a data-dependent mode with 20 dependent scans with a resolution of 60000 and
162 scan range of m/z from 350-2000. The peaks of the significant proteins were plotted directly
163 using X-calibur software™ (Thermo Fisher Scientific).

164 **Protein identification, quantitation, and GO enrichment analysis:**

165 The *Xoo*-OMV proteins were identified using Proteome Discoverer software with Sequest HT
166 and Percolator. The proteins were identified. The identification was performed with: enzyme:
167 trypsin; missed cleavage: 2; precursor mass tolerance: 10 ppm; peptide charge: +1, +2 and +3;
168 ion type: monoisotopic against the reference proteome of *Xoo*, strain KACC10331/KXO85,
169 Taxon ID. 291331, of the UniProt database. Functional annotations of *Xoo*-OMV-associated
170 proteins were designated using String Database (https://string-db.org/).

171 CR 800-PM proteins were identified, and the grouped abundances, abundance ratios, and p-
172 values of the proteins in the respective samples were quantified through label-free
173 quantification (LFQ) technique, using the consensus workflow,
174 CWF_Comprehensive_Enhanced Annotation_LFQ_and_Precursor_Quan and processing
175 workflow as PWF_Tribrid_Precursor_Quan_and_LFQ_ITHCD_CID_SequestHT_Percolator.
176 The biological, molecular functions, subcellular localisations and KEGG pathways of
177 differentially abundant proteins (DAPs) (≥1.5-fold change, $p<0.05$) were identified using
178 String Database (https://string-db.org/). Their enrichment is depicted in a lollipop graph,
179 showing strength (Log10(observed/expected)) and FDR (corrected p-values). The grouped
180 abundance of important proteins was shown in heat maps with ChiPlot (https://chiplot.online/).

181 **Ca^{2+} imaging of *Arabidopsis thaliana* Col-0 RGECO1 seedlings:**

182 4-day-old Col-0-RGECO1 seedlings were placed carefully inside a chambered slide with an
183 agar block on top and 10 µl of Ca^{2+} imaging buffer (5 mM KCl, 10 mM MES, and 10 mM
184 $CaCl_2$, pH 5.8, adjusted with TRIS) (Behera et al., 2015) was added to keep the seedlings moist
185 during imaging. 20 µl of *Xoo*-OMVs was added inside the chamber after 5 minutes of imaging.
186 The seedlings were visualized under a HC PL APO CS 10X/0.40 dry objective of Leica SP8
187 confocal microscope. The seedlings were excited at 561 nm to collect emission between 605
188 to 665 nm. The roots were imaged at an interval of 10 seconds for 30 minutes. The images
189 were analysed using ImageJ software and fractional fluorescence change, ΔF/F, was calculated
190 according to (Keinath et al., 2015). Briefly, the fluorescence intensity of each frame was
191 background corrected and normalized with the average intensity of the baseline, i.e., the first
192 five minutes as $(F-F_0)/F_0$. Three regions of interest (ROIs) were selected, ROI1- meristematic
193 region of the root; ROI2- distal elongation region of the root; ROI3- central elongation region
194 of the root. GraphPad Prism was used to draw the line curve representing the spatiotemporal
195 change in Ca^{2+} levels at individual time points (n = 6).

196 **Calcium Green 1, AM staining of rice seedlings:**

197 7-day-old Khitish and CR 800 seedlings were stained with Calcium Green1, AM, (Invitrogen)
198 (15 µM) in presence of 0.5 mg/ml phytostigmine salicylate (Sigma) for better dye loading. The
199 stained rice roots were kept inside chambered slides and covered by an agar block. 75 µl sterile
200 water was added to keep the roots moist while imaging and visualized under a Zeiss LSM800
201 confocal laser scanning microscope. The roots were excited at 488 nm at an interval of 1 minute
202 under a PLAN APO 10X dry objective with a 0.5X magnification, and emission was collected
203 in the range of 500-600 nm. After 5 minutes of imaging, 150 µl *Xoo*-OMVs was added to the
204 chambered slide. The background-corrected and normalised fluorescence intensity values
205 (ΔF/F) of the epidermis region of the root elongation zone were analysed using the ImageJ Fiji
206 software. The ΔF/F values of seedlings treated with *Xoo*-OMVs or sterile water, respectively,
207 at an interval of 5 minutes were plotted in a histogram using GraphPad Prism software. 6
208 independent experiments were compared using Student's t-test.

209 **qRT-PCR:**

210 7-day-old Khitish and CR 800 seedlings were incubated in *Xoo*-OMVs for 1 hour, followed by
211 incubation in sterile water for 1 hour (OMV) or 2 hours in sterile water (control) or pre-treated

212 with calcium chelators, BAPTA-AM (25 μM) or EGTA (2 mM) for 30 minutes, followed by
213 incubation in *Xoo*-OMVs for 1 hour then in sterile water for 1 hour. RNA was isolated from
214 the root tissue of the rice seedlings, with subsequent cDNA preparation. qRT PCR was
215 performed to quantify the expression of *PR10b* gene with the following primers: qActin-F (5′
216 ATCCTTGTATGCTAGCGGTCGA-3′), qActin-R (5′-ATCCAACCGGAGGATAGCATG-
217 3′); PR10b-F (5′-TGTGGAAGGTCTGCTTGGAC-3′), PR10b-R (5′-
218 CCTTTAGCACGTGAGTTGCG-3′) (Liu et al., 2020). Three independent replicates of the
219 experiment had been performed with each replicate consisting of 5 seedlings.

220 **Quantification of PM lipid order:**

221 7-day-old Khitish and CR 800 roots and (leaf) protoplasts, collected from the leaf tissues, were
222 treated with *Xoo*-OMVs (25 mg/ml) for 30 minutes, 60 minutes, or 90 minutes. The roots and
223 protoplasts were pre-treated with BAPTA-AM (25 μM), or EGTA (2 mM), or MβCD (2 mM)
224 (sterol-depleting agent), respectively, for 30 minutes followed by incubation in *Xoo*-OMVs as
225 mentioned. The roots and protoplasts were stained with 4 μM Di-4-ANEPPDHQ for 10 minutes
226 and viewed under a Leica SP8 confocal HC PL APO CS 60X oil immersion objective, excited
227 at 488 nm, and emission was collected at two different ranges from 500-580 nm (ordered phase)
228 and 620-750 nm (disordered phase). The GP values (+1 to -1) were calculated according to the
229 protocol of Owen et al., 2012, ($n \geq 6$).

230 **Fusion assay of OMV with FM4-64:**

231 *Xoo*-OMVs were stained with 1.5 mM FM4-64 for 10 minutes on ice in the dark. Stained *Xoo*-
232 OMVs were washed to remove any residual stain. The stained *Xoo*-OMV (FM4-64-OMV)
233 pellet was resuspended in sterile water to a concentration of 25 mg/ml, kept at 4 ^{o}C, and used
234 within 2 days. Sterile water subjected to similar staining and washing steps was used as mock
235 treatment (control). 7-day-old Khitish and CR 800 roots and leaf protoplasts were incubated
236 with FM4-64-OMVs or the mock treatment for 30 minutes, 60 minutes, or 90 minutes,
237 respectively. The seedlings were imaged under a HC PL APO CS 60X oil immersion objective
238 of Leica SP8 STED confocal microscope and excited at 568 nm, with emission collected from
239 700-795 nm. The seedlings were pre-treated with BAPTA-AM (25 μM) or EGTA (2 mM), or
240 MβCD (2 mM) for 30 minutes when mentioned, ($n \geq 7$)

241

242 **Statistical analysis:**

243 GP values and fluorescence intensity values of Fig. 3 and 4, respectively, were calculated using
244 15 ROIs from each image corresponding to individual seedlings with the help of ImageJ Fiji
245 software. The graphs, including the histograms, box plots, and line curves, were plotted to
246 visualize these values through GraphPad Prism software. One-way ANOVA was used to
247 deduce the statistical difference between the samples using GraphPad Prism software unless
248 specified. The p-value was taken as 0.05 with ns, not significant, *$P \leq 0.05$; **$P \leq 0.01$,
249 ***$P \leq 0.001$, ****$P \leq 0.0001$.

250

Results:

Xoo-OMV-associated proteins include MAMPs and virulence-associated proteins

We isolated OMVs from the BXO43 strain of *Xoo*. Through Atomic Force Microscopy (AFM) we observed that *Xoo* spontaneously releases spherical OMVs into the surroundings by blebbing (Fig. 1a, b). We determined the hydrodynamic range of the *Xoo*-OMVs using nanoparticle tracking analysis (NTA) to be 125.8 ± 1.6 nm (Fig. 1c). Transmission electron microscope (TEM) images of the *Xoo*-OMVs revealed the presence of smaller vesicles (10-60 nm) and larger vesicles (100-150 nm), indicated by a yellow and a white arrow, respectively

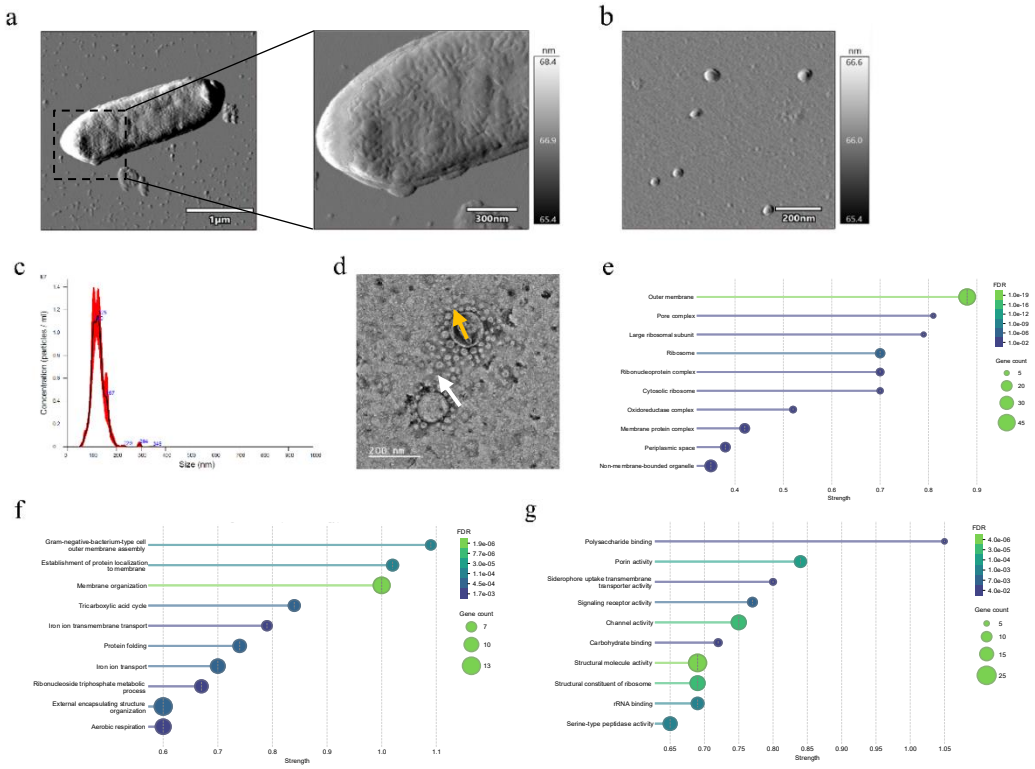

Fig. 1. Characterization of *Xoo*-OMVs and identification of their protein content. a, AFM images showing the release of BXO43 OMVs into their surroundings by blebbing. b, AFM image of spherical *Xoo*-OMVs. c, the hydrodynamic size range of the *Xoo*-OMVs (125.8 +/- 1.6 nm) exhibited by NTA. d, TEM image of *Xoo*-OMVs including smaller vesicles (10-60nm), indicated by the yellow arrow, and bigger vesicles (100-150nm), indicated by the white arrow. e, Subcellular localization of 423 proteins identified by proteomic analysis of *Xoo*-OMVs (n=4) are designated using String Database. f and g, predicted biological, and molecular functions of the proteins, appointed using String Database are represented in lollipop charts, with strength ($\log_{10}$(Expected/Observed)) in the x-axis.

259 (Fig. 1d). This corroborates with the previous reported data regarding *Xcc*-OMVs and
260 PXO99A-OMVs, which exhibit a similar size range (Bahar et al., 2016)

Table 1: Important proteins identified in Xoo-OMVs

Accession no.	Description	Gene name	Subcellular localization	Unique peptides
Pathogen/microbe-associated molecular patterns				
Q5GZN6	Flagellin	*fliC*	Extracellular	4
Q5GZN5	Flagellar hook-associated protein 2	*fliD*	Extracellular	4
Q5GZP2	Flagellar basal-body rod protein FlgG	*flgG*	Extracellular	4
Q5GZP5	Flagellar hook protein FlgE	*flgE*	Extracellular	4
Q5GZN8	Flagellar hook-associated protein 1	*flgK*	Extracellular	4
Q5GZN7	Flagellar protein	*flgL*	Extracellular	4
Q5GWR8	Elongation factor Tu	*tuf1*	Cytoplasmic	33
Q5GWS9	Elongation factor G	*fusA*	Cytoplasmic	40
Q5H1E1	Elongation factor Ts	*tsf*	Cytoplasmic	22
Cell wall-degrading enzymes				
Q5GVK0	Endoglucanase	*engXCA*	Unknown	2
Q5GU51	Predicted esterase of the alpha-beta hydrolase superfamily	*rssA*	Unknown	2
Q5H683	Cellulase	*egl*	Cytoplasmic Membrane	6
Q5GVI3	cellulase	*XOO4036*	Unknown	4
Q5H3Z0	Cellulase S	XOO1077	Extracellular	4
Q5GZB8	Polygalacturonase	pglA	Extracellular	4
Q5GXE7	Lipase esterase	*estA*	Unknown	2
Q5GVI4	Glucanase	*celA*	Extracellular	4
Other virulence-associated proteins				
Q5H6N5	VirK protein	virK	Unknown	2
Q5GWI2	3-phytase	*phy*	Unknown	2
Q5H4M4	Adhesin	*xadA*	Outer Membrane	4
Q5GZ04	Regulator of pathogenicity factors	*rpfN*	Outer Membrane	4
Q5GYV5	Aconitate hydratase B	*acnB*	Cytoplasmic	24
Q5H0Q6	Phosphoenolpyruvate synthase	*ppsA*	Cytoplasmic	18
Q5GVR9	Tail-specific protease	*prc*	Cytoplasmic Membrane	6
Q5GXA2	Phosphoglycerate kinase	*pgk*	Cytoplasmic	6
Q5GVY3	Thiol:disulfide interchange protein	*dsbA*	Periplasmic	2
Q5GV20	Outer membrane protein beta-barrel domain-containing protein	*ax21*	Outer Membrane	3
Q5H4L8	Type II secretion system core protein G	xpsG	Cytoplasmic Membrane	4
ROS protection				
Q5H243	DNA-binding ferritin-like protein (Oxidative damage protectant)	dps	Cytoplasmic	7
Q5GWL8	Transaldolase	tal	Cytoplasmic	14
Q5GU87	Superoxide dismutase [Cu-Zn]	yojM	Periplasmic	4
I1SB40	Succinate dehydrogenase flavoprotein subunit	sdhA	Cytoplasmic Membrane	6
Q5GXT8	NADH-quinone oxidoreductase	nuoG	Cytoplasmic	13
Q5GWM2	Alkyl hydroperoxide reductase C	ahpC	Cytoplasmic	18
Q5H6Y9	Enoyl-[acyl-carrier-protein] reductase [NADH]	fabV	Cytoplasmic	6
Q5GXU3	NADH-ubiquinone oxidoreductase NQO12 subunit	nuoL	Cytoplasmic Membrane	5
Q5GXT7	NADH-quinone oxidoreductase subunit F	nuoF	Cytoplasmic	8
Q5GUB3	Organic hydroperoxide resistance protein	ohr	Cytoplasmic	9
Q5H1C6	Nitrous oxidase accessory protein	NosD	Unknown	

Phosphate acquisition

Q5H5U3	Two-component system regulatory protein	*phoP*	Cytoplasmic	6
Q5H005	Phosphate-binding protein	*pstS*	Periplasmic	2
Q5H3V1	Polyphosphate-selective porin O	*oprO*	Outer Membrane	2
Q5H4B5	Inorganic pyrophosphatase	ppa	Cytoplasmic	6
Q5GZ07	Multiphosphoryl transfer protein	fruB	Cytoplasmic	11

Iron acquisition

Q5H358	Citrate-dependent iron transporter	*fecA*	Outer Membrane	3
Q5H353	Ferric enterobactin receptor	*bfeA*	Outer Membrane	3
Q5H6Z9	Iron transporter	*yncD*	Outer Membrane	3
Q5H6B6	Outer membrane receptor proteins, mostly Fe transport	*cirA*	Outer Membrane	4
Q5GUH3	Outer membrane receptor for ferrienterochelin and colicins	*fepA*	Outer Membrane	4
Q5H1Y3	TonB-dependent receptor	*iroN*	Outer Membrane	4
Q5H3W8	TonB-dependent receptor	*fyuA*	Outer Membrane	4
Q5H4B7	TonB-dependent receptor	*btuB*	Outer Membrane	4
Q5H4K6	Iron receptor	bfrC	Outer Membrane	3
Q5GV70	Bacterioferritin	*bfr*	Cytoplasmic	14

Type IV secretion system

Q5H1R3	Tfp pilus assembly protein	pilE	Unknown	2
Q5H3Q6	Fimbrial assembly protein	pilQ	Outer Membrane	2
Q5GZT4	Fimbrial biogenesis protein	pilF	Outer Membrane	3
Q5H218	Pilus biogenesis protein	pilJ	Cytoplasmic Membrane	6
Q5H3Q7	Fimbrial assembly protein	pilP	Cytoplasmic Membrane	4
Q5H2I1	Pilin	pilE	Extracellular	4

Type VI secretion system

Q5GX37	Type VI secretion system contractile sheath large subunit	XOO3480	Cytoplasmic	13
Q5GX31	Type VI secretion system tip protein	vgrG	Unknown	2
Q5GX38	Type VI secretion system tube protein	hcp	Extracellular	4
Q5GX43	Gp5/Type VI secretion system Vgr protein OB-fold domain-containing protein	VgrG	Cytoplasmic	8

Tol-Pal proteins

Q5H299	Tol-Pal system protein	tolB	Periplasmic	7
I1SB47	TolC protein	tolC	Outer Membrane	4
Q5H707	Biopolymer transport protein	exbB	Cytoplasmic Membrane	6
Q5H2A2	Tol-Pal system protein TolQ	tolQ	Cytoplasmic Membrane	6

Lipoprotein

Q5H2Q1	Predicted outer membrane lipoprotein	XOO1516	Unknown	2
Q5H2G2	Lipoprotein	XOO1605	Unknown	2
Q5H2Q6	Peptidoglycan-associated outer membrane lipoprotein	pcp	Unknown	2
Q5H3Z9	Outer membrane protein Slp	slp	Outer Membrane	4
Q5GYL4	Lipoprotein	nlpD	Outer Membrane	3
Q5GW29	Lipoprotein	LppC	Outer Membrane	3
Q5H298	Peptidoglycan-associated lipoprotein	ompP6	Outer Membrane	3
Q5H661	Lipoprotein	vacJ	Outer Membrane	3
Q5GVT2	Predicted periplasmic or secreted lipoprotein	OsmY	Periplasmic	2
Q5H2Y8	Predicted outer membrane lipoprotein	XOO1429	Unknown	2
Q5GYP5	Lipoprotein	NlpB	Unknown	2
Q5GVS8	Predicted outer membrane lipoprotein	XOO3941	Unknown	2
Q5GXI9	LPS-assembly lipoprotein LptE	rlpB	Unknown	2
Q5H5W6	Lipoprotein	XOO0400	Unknown	2
Q5H1N7	Lipoprotein	XOO1880	Unknown	2
Q5H263	Lipoprotein	XOO1704	Unknown	2

261

DSF processing proteins				
Q5H4I4	3-oxoacyl-[acyl-carrier-protein] synthase 2	fabF	Cytoplasmic Membrane	6
Q5GXJ7	Oar protein	oar	Outer Membrane	4
Q5H4C1	Ketol-acid reductoisomerase (NADP(+))	ilvC	Cytoplasmic	16
Outer membrane proteins				
Q5H1E9	Outer membrane protein assembly factor BamA	oma	Outer Membrane	4
Q5GTY7	Outer membrane protein	ompP1	Outer Membrane	4
Q5H4U1	Outer membrane protein	uptE	Outer Membrane	4
Q5GZT7	Outer membrane protein assembly factor BamB	bamB	Outer Membrane	4
Q5H4Z2	Outer membrane protein W	OmpW	Outer Membrane	3
Q5GVL3	Salt-induced outer membrane protein	XOO4006	Outer Membrane	3
Q5H3Z9	Outer membrane protein Slp	slp	Outer Membrane	3
Q5H2H1	Outer membrane protein assembly factor BamD	comL	Outer Membrane	3
Q5H4L0	General secretion pathway protein D	xpsD	Outer Membrane	3
Q5GWC2	LPS-assembly protein LptD	lptD	Outer Membrane	3
Q5H191	Outer membrane protein assembly factor BamE	smpA	Outer Membrane	3
Q5GVV7	HmsH protein	hmsH	Outer Membrane	3

We identified 290 proteins through qualitative proteomics of the proteins associated with the purified *Xoo*-OMVs, (Table S1). The identified proteins were grouped according to their functional annotations (biological, molecular functions and subcellular localisations) with the help of String Database. The proteins associated with *Xoo*-OMVs showed maximum enrichment of outer membrane proteins and pore complex proteins involved in outer membrane assembly and organisation of *Xoo* (Fig. 1e, f). Proteins involved in iron-ion transport and siderophore uptake like TonB-dependent receptors (iroN, fyuA, btuB), and iron transporters (fecA, yncD, CirA, etc) are abundant in *Xoo*-OMVs (Fig. 1g). Phosphate acquisition proteins like phoP, pstS, oprO, ppa, fruB in the *Xoo*-OMV proteome suggest the role of OMVs in nutrient acquisition (Table 1).

We report that *Xoo*-OMVs, like *Xcc*-OMVs (Bahar et al., 2016, 2014), carry known PAMPs like Ef-Tu, flagellar proteins (fliC, flgE, flgL, etc), and Ax21. Presence of other virulence-associated proteins like regulator of pathogenicity factors (rpfN), adhesins (xadA), extracellular serine protease (XOO2375), and virulence protein (virK), etc. (Table 1) imply the importance of *Xoo*-OMVs in virulence. xadA facilitates invasion through hydathodes and is crucial for optimal virulence (Das et al., 2009). XOO2375 facilitates colonization through the xylem tissue (Mendes et al., 2016). Presence of several plant-cell-wall-degrading enzymes, including cellulase (egl, XOO4036, XOO1077), endoglucanase (engXCA), esterase (estA), glucanase (celA), xylanase (xynA), etc. and secretory system proteins like T6SS proteins

283 (vgrG, hcp, XOO3480) and T4SS proteins, (including pili-forming subunits, pilE, pilQ, pilF,
284 pilJ, pilP, etc.), suggest the role of *Xoo*-OMVs in *Xoo* infection (Table 1). Moreover, *Xoo*-
285 OMVs carry proteins that facilitate defence against host immune responses (particularly against
286 ROS produced by the plants in response to OMVs), such as transaldolase, yojM, dps, organic
287 hydroperoxide resistance protein (ohr), NADH-quinone oxidoreductase proteins (nuoF, nuoL,
288 nuoG), etc. (Table 1). Overall, analysis of *Xoo*-OMV-associated proteome propose the role of
289 *Xoo*-OMVs in virulence, nutrient acquisition, invasion, colonization, and defence against the
290 host's immune response.

291 **_Xoo_-OMVs induce Ca^{2+} signal in both rice and Arabidopsis**

292 Numerous reports describe the involvement of specific Ca^{2+} signals in sensing PAMPs, such
293 as EF-Tu, chitin, and flg22, which induce a Ca^{2+} signal in plant cells (Cao et al., 2017; Keinath
294 et al., 2015; Ranf et al., 2014). The identification of these MAMPs in the *Xoo*-OMV-associated
295 proteome drove us to examine whether *Xoo*-OMVs induce any Ca^{2+} signal in plant cells. To
296 accomplish this, we used a Ca^{2+}-indicator stain, Calcium Green1, AM, to stain CR 800
297 (resistant variety) and Khitish (susceptible variety) seedlings, respectively. Rice leaves are
298 hydrophobic and difficult to stain; as an alternative, we imaged rice roots, as they serve as the
299 entry point for *Xoo* infection through contaminated irrigation water and soil (Naqvi, 2019). We
300 observed an increase in Ca^{2+} concentration (depicted by the false colour code, calculated as
301 ΔF/F) in the epidermal cells of the root distal elongation zone of both Khitish and CR 800 after
302 10 minutes of *Xoo*-OMV treatment (Fig. 2a, b). No elevation of Ca^{2+} concentration was
303 observed in the roots treated with sterile water. ΔF/F values of each seedling treated with sterile
304 water (control) or *Xoo*-OMVs (OMV) at specific time points were plotted in a histogram for
305 comparison (Fig. 2c, d). Six independent imaging experiments were carried out for each
306 variety.

307 To further visualize the spatiotemporal propagation of the *Xoo*-OMV-induced Ca^{2+} signals we
308 used transgenic Arabidopsis Col-0 seedlings expressing the genetically encoded Ca^{2+} indicator
309 RGECO1 as the system. We placed 4-day-old Col-0-RGECO1 seedlings in custom-made
310 chambered slides, and performed live-cell imaging as described in the Material and Methods.
311 The seedlings were imaged for 5 minutes in solvent control to obtain a stable baseline, and then
312 20 µl of 100 mg/ml *Xoo*-OMVs was added to the chamber containing the seedling. We
313 observed a gradual Ca^{2+} signal with an amplitude of 0.5 (ΔF/F) after 10 minutes of purified
314 *Xoo*-OMV application (Fig. 2e, g). To analyse the observed signal, we defined three ROIs

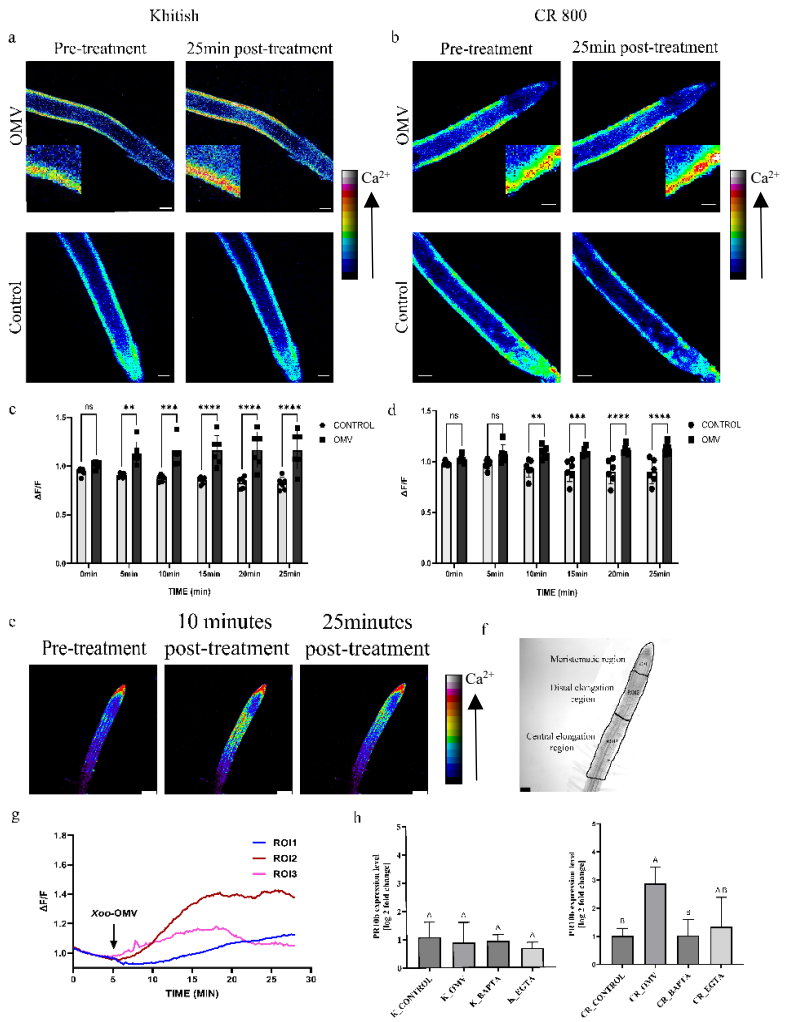

Fig. 2. *Xoo*-OMVs induce cellular Ca^{2+} elevation in rice and Arabidopsis roots. a and b, 7-day-old Khitish and CR 800 roots, respectively, stained with Calcium Green1, AM, showing an increase in cellular Ca^{2+} when treated with *Xoo*-OMVs. No Ca^{2+} elevation was observed with solvent treatment, scale bar=125 µm. c and d, the relative fluorescence of the Khitish and CR 800 roots after treatment with *Xoo*-OMVs and solvent control were plotted as a histogram at intervals of 5 minutes using GraphPad Prism software (n=6). Student's t-test was done to deduce the statistical difference between the fluorescence of control and *Xoo*-OMV-treated roots at each time point, n=6. e, 4-day-old Arabidopsis Col-0 roots, expressing Ca^{2+} indicator protein RGECO1 treated with *Xoo*-OMVs. showing an increase in fluorescence, indicating a Ca^{2+} spike after treatment with *Xoo*-OMVs, scale bar=50 µm. f, selection of ROIs, namely, the meristematic region (ROI1), the distal elongation region (ROI2), and the central elongation region (ROI3). g, the average line curve (n=5) showing the Ca^{2+} signal induced by *Xoo*-OMVs in different ROIs of the Arabidopsis roots with respect to time. The black arrow indicates the time of application of *Xoo*-OMVs. h, the relative expression of the *PR10b* gene after incubation in *Xoo*-OMVs for 1 hour (in the presence and absence of Ca^{2+}-chelator) in CR 800 and Khitish roots, (n=3 independent replicates). The statistical differences have been calculated through one-way ANOVA using GraphPad Prism software (ns, not significant, *P≤0.05; **P≤0.01, ***P≤0.001, ****P≤0.0001).

around three distinct regions of the root, namely, the meristematic region (ROI1), the distal elongation region (ROI2), and the central elongation region (ROI3) (Fig. 2f). The increase in

317 the Ca^{2+} concentration was most prominently displayed in the distal elongation zone of the root
318 (Fig. 2e, g). In conclusion, *Xoo*-OMVs can induce a Ca^{2+} signal in both the host rice and non-
319 host Arabidopsis within 10 minutes of exposure.

320 To investigate whether the early Ca^{2+} signal is necessary for the OMV-induced immune
321 response in host plants, we treated 7-day-old Khitish and CR 800 seedlings with *Xoo*-OMVs
322 for 1 hour, with or without pre-treatment with Ca^{2+}-chelators (BAPTA or EGTA), as described
323 in the Materials and Methods. We observed that the resistant variety of rice, CR 800, could
324 exhibit an immune response against *Xoo* after treatment with *Xoo*-OMVs, indicated by a three-
325 fold elevation in the expression of *PR10b gene* compared to the incubation in sterile water. On
326 the other hand, Khitish, the susceptible variety of rice, could not evoke any such immune
327 response after exposure to *Xoo*-OMVs (Fig. 2h). Further, the immune response displayed by
328 CR 800 was weakened in a Ca^{2+}-deprived condition, indicated by the reduced expression of
329 *PR10b* (Fig. 2h). These results suggest that the early Ca^{2+} signal triggered by *Xoo*-OMVs is
330 crucial for the perception of *Xoo*-OMVs and activation of downstream immune response
331 against *Xoo* in CR 800.

332 ***Xoo-OMVs* instigate rapid nanodomain enrichment in rice in a Ca^{2+}-dependent manner**

333 It has been reported that the fusion of *Xcc*-OMVs with the PM of Arabidopsis leads to an
334 increase in the membrane order (Tran et al., 2022). We inspected whether *Xoo*-OMVs can exert
335 similar effect on rice PM. Furthermore, we investigated the role of Ca^{2+}signal generated by
336 *Xoo*-OMVs in changing the membrane order. We used Di-4-ANEPPDHQ, a polarity-sensitive
337 membrane dye (Owen et al., 2012), to assess the state of lipid order of rice PM in the presence
338 of *Xoo*-OMVs. Di-4-ANEPPDHQ shows a spectral shift of 60 nm between disordered and
339 ordered phases of the membrane. The lipid order of the membrane can be quantified using the
340 generalised polarity (GP) values, which range from -1 to +1, indicating the polarity of the
341 membrane and thereby suggesting the order of the membrane. Higher GP values correspond to
342 a highly ordered membrane or a nanodomain-rich membrane (Owen et al., 2012).

343 We found that after 30 minutes of incubation in *Xoo*-OMVs, the roots of 7-day-old Khitish and
344 CR 800 seedlings showed a significant increase in the GP value of the PM ($P \leq 0.0001$, $n \geq 6$
345 seedlings), compared to roots incubated in sterile water (control) (Fig. 3a, b), indicating a
346 highly ordered membrane (Fig. 3a, b). The increased order of the PM was maintained for up to
347 90 minutes of *Xoo*-OMV treatment (Fig. S1). Conversely, Khitish and CR 800 seedlings pre-

348 treated with EGTA or BAPTA-AM for 30 minutes exhibited a reduced increase in the lipid
349 order of the PM after 30 minutes of incubation. *Xoo*-OMVs (Fig. 3a, b).

350 We examined whether *Xoo*-OMVs had an analogous effect on the PM of the leaf tissue as well.
351 As it was difficult to stain rice leaves due to their hydrophobic nature, we isolated protoplasts
352 from Khitish and CR 800 leaves and incubated the protoplasts with *Xoo*-OMVs for 30 minutes.
353 The protoplasts stained with Di-4-ANEPPDHQ (3.5 µM) were mounted on a chambered slide
354 for visualisation. The protoplasts incubated with *Xoo*-OMVs displayed significantly higher GP
355 values than the protoplasts incubated with sterile water (control) (Fig. 3c). Similar to the rice
356 roots, leaf protoplasts also displayed a compromised increase in the lipid order of the PM after
357 Ca^{2+}-chelation with BAPTA-AM (25 µM) (Fig. 3c, d). In order to verify that the rise of the

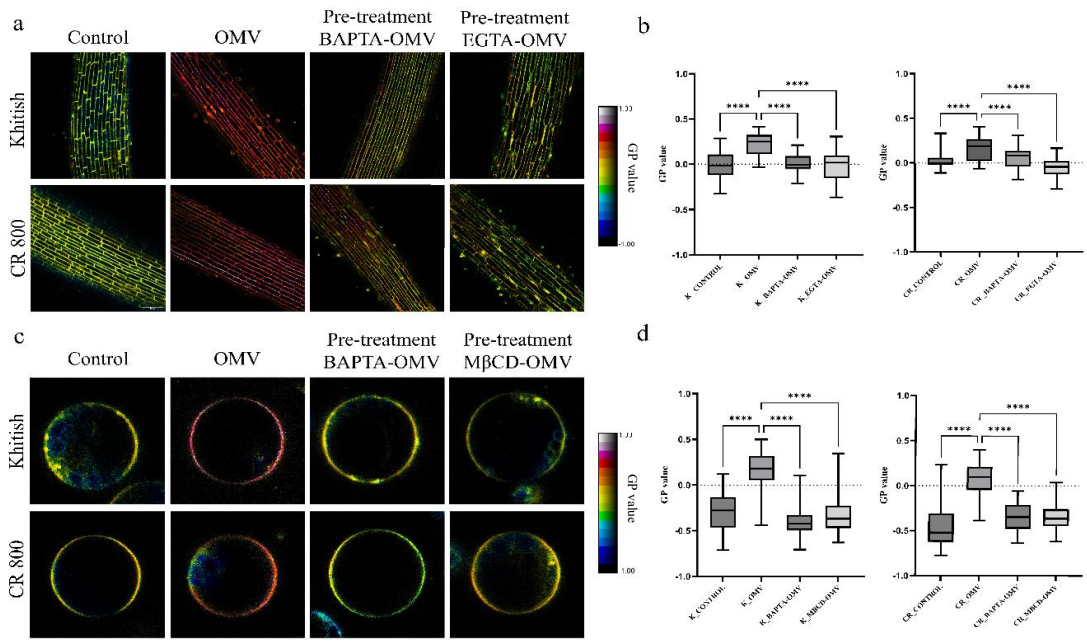

Fig. 3 Ca^{2+} and sterol-dependent lipid order increase in rice PM after incubation in *Xoo*-OMVs. a, 7-day-old Khitish and CR 800 roots incubated with *Xoo*-OMVs for 30 min and stained with Di-4-ANEPPDHQ showing an increase in the lipid order of rice PM (n≥6 seedlings). 30-minute pre-treatment with BAPTA-AM (25 µM) or EGTA (2 mM) inhibits lipid order increase. b, GP values (-1 to +1) have been calculated using ImageJ software and plotted in a Box-plot using GraphPad Prism software, the corresponding statistical significance have been calculated through one-way ANOVA (p≤0.05), c, leaf protoplasts isolated from Khitish and CR 800 showing lipid order rise after incubation with *Xoo*-OMVs. BAPTA-AM (25 µM) or MβCD (2 mM) pre-treated protoplasts not showing significant rise in lipid order even after *Xoo*-OMV exposure. d, GP values of the protoplast membrane of Khitish and CR 800, represented in a box plot. The statistical significance has been calculated by one-way ANOVA using GraphPad Prism software (ns, not significant, *P≤0.05; **P≤0.01, ***P≤0.001, ****P≤0.0001).

lipid order of the host membrane is due to nanodomain enrichment, and not merely a biophysical effect, we treated the rice leaf protoplasts with MβCD (2 mM), a sterol-depleting agent. Protoplasts pre-treated with MβCD showed no increase in lipid order upon incubation in *Xoo*-OMVs for 30 minutes (Fig. 3c). The GP values (+1 to -1) of the respective experiments have been plotted in a box plot, and their statistical differences have been calculated using one-way ANOVA with the help of GraphPad Prism software (Fig. 3b, d). Collectively, our observations suggest that the early Ca^{2+} signal is necessary for *Xoo*-OMV-induced nanodomain enrichment in the rice PM.

Incorporation of *Xoo*-OMVs in rice PM is Ca^{2+}-dependent and nanodomain-mediated

OMVs can enter the non-phagocytic host cells through various pathways, especially in a cholesterol-dependent lipid raft-mediated way (Kaparakis-Liaskos and Ferrero, 2015; Schaar et al., 2011). *Xcc*-OMVs get incorporated into the Arabidopsis PM in a sterol-dependent manner (Tran et al., 2022). Accordingly, we investigated the insertion of *Xoo*-OMVs in rice

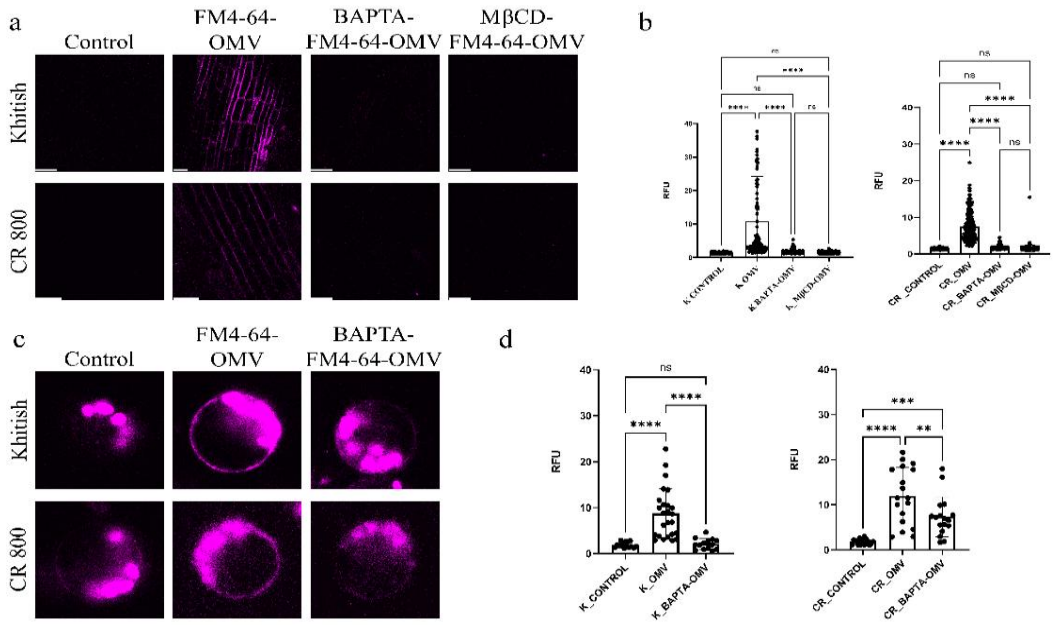

Fig. 4. *Xoo*-OMVs get inserted into rice PM. a, 7-day-old Khitish and CR 800 roots showing a significant decrease in *Xoo*-OMV insertion on Ca^{2+}-chelation and sterol-depletion with BAPTA-AM (25 µM) and MβCD (2 mM), respectively (n≥7 seedlings), scale bar=20 µm. b, histogram showing the statistical difference between the relative fluorescence units of each sample, calculated using one-way ANOVA by GraphPad Prism. c, FM4-64 stained *Xoo*-OMVs inserted into the PM of leaf protoplasts with and without pre-treatment with BAPTA-AM (25 µM). d, GraphPad Prism was used to create the histograms and analyse the statistical difference between the protoplast samples through one-way ANOVA, (ns, not significant, *P≤0.05; **P≤0.01, ***P≤0.001, ****P≤0.0001).

371 PM and its Ca^{2+} dependency. Similar to the aforementioned paper, we used FM4-64, a
372 lipophilic dye, to stain the *Xoo*-OMVs, allowing us to track them. *Xoo*-OMVs were stained as
373 described in Materials and Methods (Fig. S2a). The fluorescence of FM4-64 was checked
374 through confocal laser scanning microscopy to visualize the localization of FM4-64-*Xoo*-
375 OMVs in the plant tissue. Roots of 7-day-old Khitish and CR 800 seedlings were incubated in
376 FM4-64-*Xoo*-OMVs and the mock treatment (control). After 30 minutes of incubation in FM4-
377 64-*Xoo*-OMVs, the PM of rice roots showed slight fluorescence, indicating the initiation of
378 fusion of the *Xoo*-OMVs with the rice PM. After 60 minutes or 90 minutes of incubation, the
379 fluorescence in the roots incubated in FM4-64-*Xoo*-OMVs increased considerably, indicating
380 the incorporation of *Xoo*-OMVs into the rice root PM. No fluorescence was observed in the
381 PM of the rice roots incubated in the mock treatment, confirming that the remnant dye was
382 insignificant (Fig. S2c). The fluorescence detection range of FM4-64 is close to that of
383 chloroplasts. Thus, to visualize the membrane of the leaf tissues clearly without
384 misinterpretation due to the auto-fluorescence of the chloroplasts, we used protoplasts isolated
385 from the rice leaf tissues as the system for this experiment. Protoplasts, isolated from the leaves
386 of Khitish and CR 800, were incubated with either FM4-64-*Xoo*-OMVs or the mock treatment.
387 The protoplasts that distinctly showed the PM were chosen for analysis. The ROI was selected
388 from the bright field images on the regions showing the PM (Fig. S2b). It was noticed that like
389 in the roots, the FM4-64-*Xoo*-OMVs were incorporated into the PM of the protoplasts after 60
390 minutes of incubation (Fig. 4c).

391 We further checked whether the initial Ca^{2+} signal in the host and the subsequent increase in
392 lipid order of the host membrane are necessary for the incorporation of *Xoo*-OMVs into the
393 rice PM. On chelation of intracellular Ca^{2+} with BAPTA, the insertion of *Xoo*-OMVs in the
394 rice root PM was significantly reduced (Fig. 4a, b). The protoplasts pre-treated with BAPTA
395 manifested a similar decrease in the insertion of *Xoo*-OMVs into the rice PM (Fig. 4c, d). Roots
396 of Khitish and CR 800 seedlings pre-treated with MβCD for 30 minutes displayed no fusion of
397 *Xoo*-OMVs with the rice PM (Fig. 4a, b). Taken together, our data demonstrate that the
398 integration of *Xoo*-OMVs into rice PM is a Ca^{2+}-dependent and nanodomain-mediated process.

399 **Ca^{2+} is crucial for the enrichment of defence-related proteins in the PM of CR 800 after**
400 ***Xoo*-OMV treatment**

401 The composition of PM proteins is modulated according to the cell's state, which helps the
402 cell recognise and respond to various abiotic and biotic stimuli (Cao et al., 2016; Fujiwara et

403 al., 2009; Komatsu, 2008). An increase in the abundance of defence-related proteins involved
404 in ABA signalling, ROS bursts, SA signalling, etc., is observed in the rice PM after exposure
405 to Magnaporthe oryzae (Cao et al., 2016) and Xoo (Chen et al., 2007; Fujiwara et al., 2009).

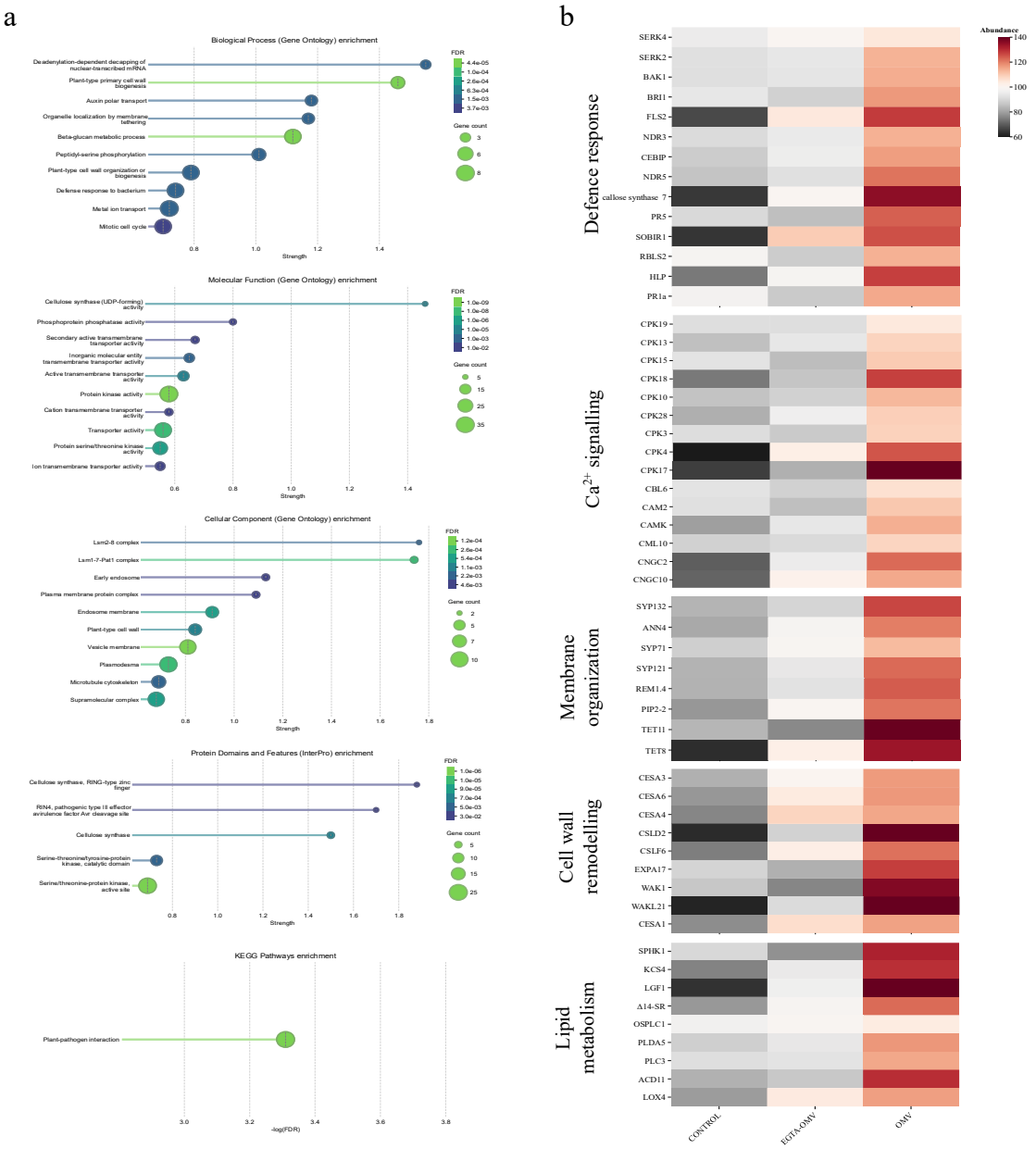

Fig. 5. Analysis of the CR 800 PM proteome remodelling after *Xoo*-OMV treatment in native and Ca^{2+}-deprived condition. a, Functional annotations of the 233 proteins upregulated (1.5≥Fold-change, p≤0.05) in CR 800 PM after *Xoo*-OMV treatment in normal condition, but not in a Ca^{2+}-chelated condition. Enrichment is represented as a lollipop chart created using String Database with strength (log_{10}(Expected/Observed)) in the x-axis. b, Heatmap displays the abundance of key proteins involved in important pathways as observed after different treatments, Control (sterile water-1hr), EGTA-OMV (30 min pre-treatment with EGTA (2mM); *Xoo*-OMV-1hr), and OMV (*Xoo*-OMV-1hr), (n=3).

406 We examined whether Xoo-OMV-induced increase in lipid order mobilises the assembly of
407 specific proteins in the rice PM. To this end, we carried out a quantitative proteomic analysis
408 of membrane proteins from the CR 800 variety, as CR 800 can mount an immune response
409 against Xoo. Specifically, 7-day-old CR 800 seedlings were incubated in Xoo-OMV or sterile
410 water, or pre-treated with EGTA (2 mM) for 30 minutes before incubation in Xoo-OMV for 1
411 hour. The PM fraction was enriched using the protocol of Uemura et al. (1995). PM proteins
412 were analysed by label-free quantification (LFQ). A total of 3274 proteins were identified; of
413 these, 2689 proteins were present in all sample groups (Control, EGTA-OMV, and OMV),
414 while 54 were exclusively associated with the PM of roots treated with Xoo-OMVs. We
415 found that approximately 430 proteins were upregulated (≥1.5-fold change, $p>0.05$) in OMV-
416 treated roots, while 351 proteins were upregulated in EGTA-OMV treated roots.
417 Furthermore, through functional annotations we found that proteins that were upregulated
418 after Xoo-OMV treatment were predominantly involved in cell wall biogenesis, vesicle
419 docking, Ca2+ signalling, and most importantly, in defence against bacteria. None of the
420 above-mentioned signalling pathways were enriched under Ca2+-chelated conditions.

Table 2: Important proteins found in CR 800 PM with their respective Abundance ratios

DESCRIPTION	GENE ID	ABUNDANCE: EGTA-OMV/CONTROL	ABUNDANCE: OMV/CONTROL
Calcium signalling proteins			
Calcium-dependent protein kinase 19, CPK19	Os07g0515100	1.028	1.216
Calcium-dependent protein kinase 13, CPK13	Os04g0584600	1.107	1.36
Calcium-transporting ATPase 5, plasma membrane-type, ACA5	Os04g0605500	0.939	1.192
Calcium-dependent protein kinase 8, CPK8	Os03g0808600	0.961	1.21
Sodium/calcium exchanger, NCL1	Os01g0212400	1.154	1.324
Calmodulin-2, CAM2	Os05g0491100	0.937	1.228
Calcium-dependent protein kinase 18, CPK18	Os07g0409900	1.317	1.87
Calcium-dependent protein kinase 10, CPK10	Os03g0788500	0.942	1.363
Calcium-dependent protein kinase 28, CPK28	Os12g0169800	1.187	1.473
Calcium-dependent protein kinase 4, CPK4	Os02g0126400	1.861	1.998
Calcium/calmodulin-dependent serine/threonine-protein kinase 1, CAMK1	Os03g0366200	1.175	1.324
Probable calcium-binding protein, CML10	Os01g0949500	1.127	1.48
Calcium-dependent protein kinase 17, CPK17	Os07g0161600	1.278	2.85
Cyclic nucleotide-gated calcium channel, CNGC2	Os02g0255000	0.887	1.384
Cyclic nucleotide-gated calcium channel, CNGC9	Os09g0558300	1.229	1.546
Cyclic nucleotide-gated calcium channel, CNGC10	Os02g0789100	1.466	1.648

421

DEFENCE RELATED PROTEINS:			
RPM1 Interacting Protein 4	Os04g0379600	0.98	1.231
LRR receptor kinase, SERK2	Os04g0457800	1.129	1.57
LRR receptor kinase, SERK4	Os02g0283800	1.073	1.605
SOBIR1	Os06g0288100	1.355	4.289
RIN4 Domain Containing Protein	Os08g0526400	1.391	1.558
Protein phosphatase 2C 35, XB15	Os03g0821300	1.628	1.723
HVA22-like protein, HLP	Os11g0156600	1.375	2.366
HVA22-like protein, HLP	Os12g0158600	0.678	1.333
Callose Synthase 7	Os02g0832500	1.47	2.366
Chitin Elicitor Binding Protein, CEBiP	Os09g0548200	1.116	1.333
LRR receptor kinase, BAK1	Os08g0174700	1.024	1.434
Brassinosteroid LRR receptor kinase, BRI1	Os01g0718300	0.827	0.863
Harpin-induced 1 domain-containing Protein	Os06g0163300	1.257	1.592
Hypersensitive-induced response protein-like protein 2, HIRL2	Os09g0361200	0.975	1.133
Hypersensitive Immune Response Induced Protein	Os01g0588100	1.173	1.726
Leaf Rust 10 Disease-resistance locus receptor-like protein kinase-like 1.2	Os05g0550800	1.26	1.699
Nucleotide-Binding Site – Leucine-Rich Repeat protein, NBS-LRR	Os11g0227100	0.01	1.669
Harpin induced protein 5, NDR5	Os04g0685400	1.104	1.457
Nitrate Transporter, NRT1	Os10g0579600	0.603	1.594
LRR receptor-like serine/threonine-protein kinase, FLS2	Os04g0618700	1.372	1.47
Pathogenic type III effector avirulence factor Avr cleavage site domain containing protein	Os03g0169900	1.12	2.165
Pathogenesis-Related protein, PR1alpha	Os10g0191300	0.931	1.122
Pathogenesis-Related protein, PR5	Os03g0661600	0.868	1.077
Resistance to bacterial leaf streak 2, RBLS2	Os02g0543000	0.92	1.516
E3 ubiquitin ligase, OsRGLG5	Os06g0608800	1.309	1.526
Plant intracellular Ras-group-related LRR protein 6, IRL6	Os02g0826600	0.844	3.434
Dirigent protein	Os12g0228700	1.653	2.344
Dirigent protein	Os10g0334500	1.282	2.908
RECEPTOR-like kinases			
L-type lectin-domain containing receptor kinase SIT2-like protein	Os03g0772600	1.122	1.449
Probable L-type lectin-domain containing receptor kinase S.5	Os02g0712600	1.245	2.01
Leucine rich repeat-containing RLK, LRR-RLK	Os11g0249900	0.952	1.376
Leucine rich repeat-containing RLK, LRR-RLK	Os05g0480400	1.472	2.285
Leucine rich repeat-containing RLK, LRR-RLK	Os01g0818700	1.484	1.817
Leucine rich repeat-containing RLK, LRR-RLK	Os05g0524500	0.688	1.393
Leucine rich repeat-containing RLK, LRR-RLK	Os08g0203201	1.246	1.697
Leucine rich repeat-containing RLK, LRR-RLK	Os05g0525400	1.053	1.716
Receptor-like cytoplasmic kinase, RLCK 277	Os09g0513600	0.946	1.266
Receptor-like cytoplasmic kinase, RLCK 277	Os02g0513000	1.149	1.505
Receptor-like cytoplasmic kinase RLCK176	Os05g0110900	1.496	1.649
Malectin Receptor like Kinase, CrRLK15	Os05g0493100	1.09	1.66
Malectin Receptor like Kinase, CrRLK1L15	Os06g0334300	0.951	1.295

422

MEMBRANE ORGANIZATION			
Ankyrin repeat-containing protein	Os02g0810100	1.228	1.667
Annexin	Os09g0394900	1.109	1.385
Probable aquaporin, PIP2-2	Os02g0629200	1.317	1.674
Aquaporin, PIP2-5		0.84	1.295
Remorin 1.4, REM1.4	Os02g0642200	1.194	1.804
Remorin 4.1, REM4.1	Os07g0569100	1.417	1.65
RHOMBOID-like protein, RLP2	Os04g0569300	1.163	1.716
Syntaxin, SYP131	Os06g0168500	1.106	1.806
Syntaxin 121, SYP121	Os03g0787000	1.278	1.638
Syntaxin, SYP71	Os05g0553700	1.056	1.326
Tetraspanin, TET11	Os08g0260600	0.966	1.578
Tetraspanin, TET8	Os09g0425900	1.634	1.969
CELL WALL REMODELLING			
Probable cellulose synthase A catalytic subunit 1, CESA1	Os05g0176100	1.462	1.565
Probable cellulose synthase A catalytic subunit 8, CESA8	Os07g0208500	1.452	1.614
Probable cellulose synthase A catalytic subunit 6, CESA6	Os07g0252400	1.402	1.63
Cellulose synthase A catalytic subunit 4, CESA4	Os01g0750300	1.363	1.93
Probable mixed-linked glucan synthase 6, CSLF6	Os08g0160500	1.444	1.674
Cellulose synthase-like protein D2, CSLD2	Os06g0111800	1.863	1.903
Endoglucanase 12, GLU3	Os04g0497200	1.064	1.508
Wall-associated kinase like protein 21, WAKL21	Os12g0595800	1.119	1.821
Wall-associated kinase, WAK1	Os01g0136400	0.801	1.349
Pectinesterase	Os06g0104300	1.306	1.587
Wall-associated kinase, WAK10a	Os01g0689900	1.004	1.22
Pectinesterase	Os01g0100400	1.064	1.507
Wall-associated kinase, WAK2	Os10g0162844	1.093	1.586
LIPID METABOLISM			
Phospholipase D, PLD	Os06g0604200	1.141	1.411
Phosphoinositide phospholipase C, PLC1	Os12g0562400	0.911	1.183
Squalene synthase	Os03g0805100	0.911	11.119
Acyl-CoA-binding domain-containing protein 2, ACBP2	Os06g0115300	0.463	1.85
3-ketoacyl-CoA synthase, KCS4	Os05g0568000	1.296	1.694
Probable linoleate 9S-lipoxygenase 4	Os03g0700700	1.456	1.677
CDP-diacylglycerol--inositol 3-phosphatidyltransferase	Os02g0123600	0.01	1.507
Acceleration of cell death, ACD11	Os08g0556300	1.073	1.56
Phospholipid-transporting ATPase	Os05g0100600	1.145	1.566
Sphingosine Kinase 1	Os07g0563000	0.854	1.27
Hydroxysteroid dehydrogenase, LGF1	Os11g0499600	1.596	2.552

423 We identified 233 proteins that were significantly upregulated (≥1.5-fold change, p>0.05) in
424 CR 800 roots in response to *Xoo*-OMVs, but not under a Ca^{2+}-deprived condition. Through
425 functional annotation analysis of the these differentially abundant proteins (DAPs) using String
426 Database, we found that these proteins are majorly responsible for plant cell wall remodelling
427 and biogenesis (WAK2, WAKL21, CESA6, CESA4, CSLF6, etc.) (Li et al., 2009; Malukani
428 et al., 2020), receptor-like kinases (LRR-RLKs, RLCKs and lectin domain containing kinases
429 etc.) (Mou et al., 2024; Yang et al., 2020), Ca^{2+} signalling proteins (CPK18, CPK17, CML10,
430 CNGC9 etc.) (Bundó and Coca, 2017; Wang et al., 2019), defence response-related proteins
431 (SERK2, NRT1, RBLS2, RGLG2 IRL6, etc.) (Liu et al., 2023), and lipid metabolism proteins
432 (PLD, ACBP2, KCS, etc.) (Kim et al., 2013; Young et al., 1996) (Fig. 5a). Interestingly, we
433 observed that microdomain-associated proteins, like remorins (REM1.4 and REM4.1) (Gui et
434 al., 2016), syntaxins (SYP121 and SYP71) (Bao et al., 2012; Cao et al., 2019), tetraspanins
435 (TET8 and TET11), aquaporins (PIP2-2 and PIP2-5), and annexin are more abundant in OMV-
436 treated roots than in EGTA-OMV-treated roots. Moreover, proteins that positively regulate
437 resistance against *Xoo*, like, HVA22-like proteins, leaf rust resistance protein, RBLS2,
438 RGLG5, etc. and hypersensitive response proteins like PR1a, PR5, callose synthase, dirigent
439 proteins (Paniagua et al., 2017), HIRL2, etc. were also reduced under a Ca^{2+}-chelated condition
440 (Fig. 5b; Table 2). Notably, the abundance of immune co-receptors, playing a key role in
441 defence against *Xoo*, like, SERK2, SOBIR1, BAK1 and BRI1 (Chen et al., 2014; Zhang et al.,
442 2021) are elevated in CR 800 PM proteome following treatment with *Xoo*-OMVs in presence
443 of Ca^{2+}, but not in Ca^{2+}-deprived condition (Fig. 5b). These outcomes are consistent with our
444 previous findings, which demonstrate that *Xoo*-OMV-induced nanodomain enrichment and
445 immune response are impaired in a Ca^{2+}-chelated condition.

446 **Discussion:**

447 Gram-negative bacteria utilise outer membrane vesicles (OMVs) to enhance their chances of
448 survival within the host, concurrently, the host has evolved to recognise OMVs and mount an
449 immune response against the invading pathogen to protect itself (McMillan and Kuehn, 2021;
450 Schwechheimer and Kuehn, 2015). Emerging evidence depicts the function of phytopathogenic
451 OMVs in plant-pathogen interactions. In Arabidopsis, *Xcc*-OMVs potentiate an immune
452 response via nanodomain-mediated insertion of the OMVs into the plant PM (Bahar et al.,
453 2016; Tran et al., 2022). Additionally, pre-treatment with OMVs, like *Pst*-OMVs in tomato
454 plants or *Xcc*-OMVs in Arabidopsis, can protect the plant from subsequent infection

455 (Chalupowicz et al., 2023; McMillan and Kuehn, 2023). Nevertheless, the molecular
456 mechanism and sequence of events that lead plants to mount an immune response after
457 recognising pathogenic OMVs are still unknown.

458 Our study aimed to uncover the initial signalling events through which rice perceives *Xoo*-
459 OMVs. We have isolated and categorised the proteins associated with *Xoo*-OMVs to find
460 several MAMPs, virulence-associated proteins, secretory system proteins, DSF-processing
461 enzymes, and hydrolytic enzymes, which indicate the role of *Xoo*-OMVs during invasion and
462 pathogenesis inside the host (Fig. 1, Table 1). We found that several cell wall-degrading
463 enzymes like cellulase, endoglucanase, esterase, etc. (Table 1) are associated with *Xoo*-OMVs,
464 which destabilise the cell wall of the plant to enable the insertion of OMVs in the PM.
465 Meanwhile, cell wall degradation produces DAMPs that can alert the host. Performing
466 quantitative proteome analysis of CR 800 roots, we observed an increase in the abundance of
467 chitin elicitor binding protein (CEBiP) that recognises the cell wall-derived oligosaccharides
468 as DAMPs (Fig. 5b) to mount an immune response (Yang et al., 2021). Interestingly, *Xoo*-
469 OMV-treated rice proteome shows increased abundance of (i) cell wall-remodelling enzymes
470 (endoglucanase, pectinesterase, WAKs) to produce more DAMPs and amplify the immune
471 response and modify the cell wall, and (ii) cell wall biosynthesis enzymes (CESAs, CSFL6) to
472 repair the damaged cell wall. *Xoo*-OMVs contain iron and phosphate channels (Table 1) to
473 ensure optimum virulence (Chatterjee et al., 2003; Subramoni et al., 2012). We also observed
474 an increase in abundance of several metal ion transporters in rice root PM after *Xoo*-OMV
475 treatment, suggesting a probable competition for available nutrients between the plant and the
476 pathogen (Fig. 5a). The proteins carried by the *Xoo*-OMVs reflect that OMVs consist of
477 numerous proteins that not only enhance virulence of *Xoo* but also defend the bacteria against
478 plant's immune responses and promote the chance of survival inside the host. At the same time,
479 the plant recognizes the OMVs and responds by recruiting necessary proteins in its PM.

480 MAMPs, such as flg22 and elf18, are known to induce Ca^{2+} signals in Arabidopsis (Ranf et al.,
481 2014). We have observed that, *Xoo*-OMVs which carry a complex cocktail of MAMPs, induces
482 a gradual Ca^{2+} signal in the elongation zone of the rice root after 10 minutes of *Xoo*-OMV
483 application. Live cell Ca^{2+} imaging with Arabidopsis Col-0-RGECO1 seedlings revealed that
484 the spatiotemporal resolution of the signal is unique compared to other individual MAMPs
485 (Fig. 2). OMVs consist of lipopolysaccharides and MAMPs like flg22, EF-Tu, extracellular
486 peptidase, cellulase, and other extracellular secretion system proteins (Table S1), the Ca^{2+}

signals that we have observed is not specific to any particular MAMP; rather, it is a response of the root cells towards a mixture of MAMPs. Our results demonstrate that this rapid Ca^{2+} signal is the key to *Xoo*-OMV perception by rice, and alongside ROS serves as another hallmark of OMV perception by plants.

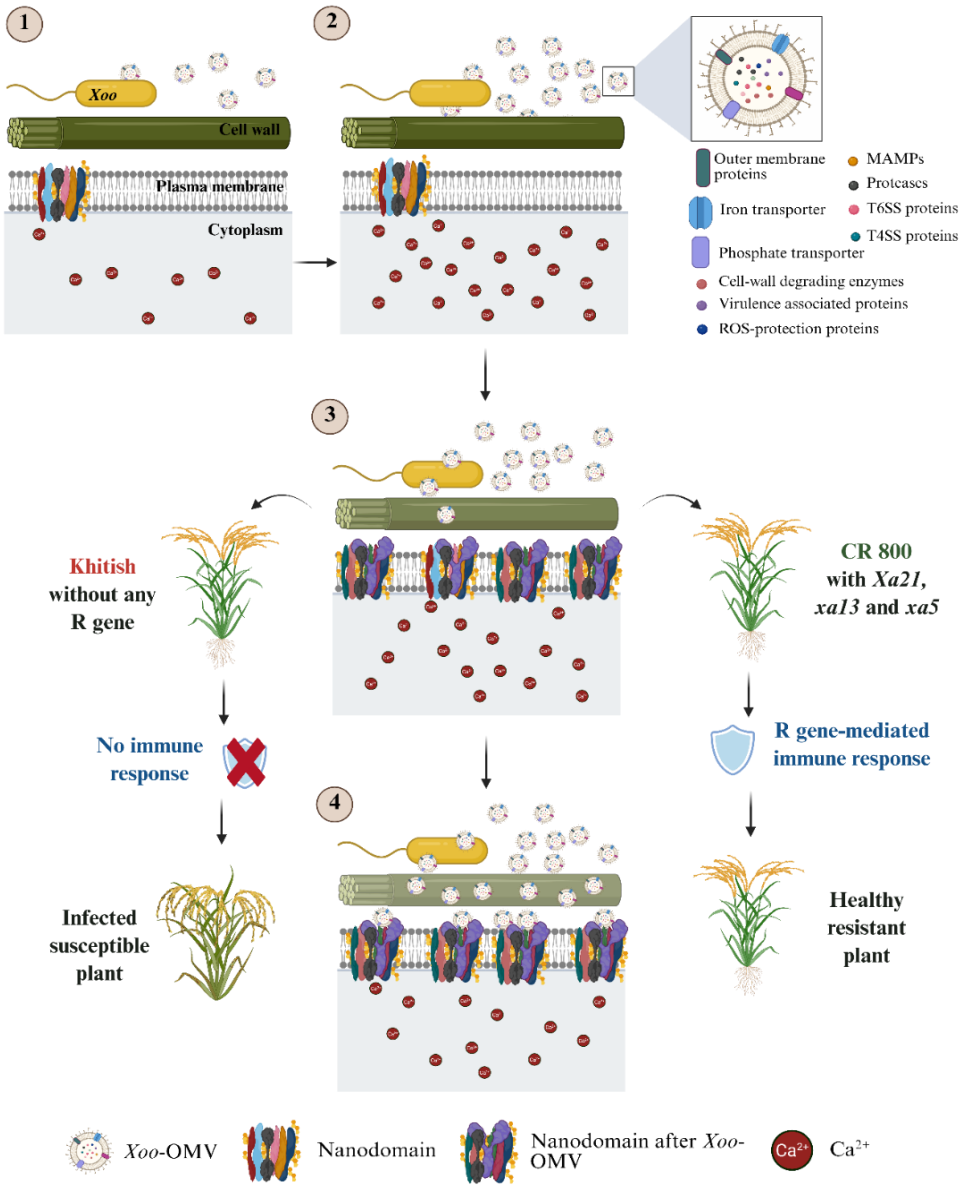

Fig. 6. Ca^{2+}-dependent perception of *Xoo*-OMVs by rice via nanodomain-mediated PM proteome reorganization. *Xoo*-OMVs are associated with MAMPs and virulence-associated proteins. Through these MAMPs, the rice cell recognizes the *Xoo*-OMVs by evoking a Ca^{2+} signal. This leads to nanodomain enrichment in the rice PM and shifts the PM proteome towards the defence response pathway. It also enables insertion of *Xoo*-OMVs into the rice PM. Both Khitish and CR 800 perceive the *Xoo*-OMVs similarly, but, the resistant variety CR 800, expressing R genes (*Xa21*, *xa13, xa5*) mounts an immune response against the pathogen, while Khitish the susceptible variety without any R gene cannot evoke any immune response. If the early Ca^{2+} signal is blocked, *Xoo*-OMV perception and following immune response are impaired in CR 800.

491 It is well-established that plant pathogen-derived OMVs can trigger an immune response in the
492 host plant (Bahar et al., 2016; Chalupowicz et al., 2023; McMillan et al., 2021). CR 800
493 (expressing *Xa21, xa3*, and *xa15*) can display a significant immune response against *Xoo*-
494 OMVs, while Khitish (expressing no R genes) is susceptible to *Xoo* infection and cannot mount
495 any immune response against *Xoo*-OMVs. These results are consistent with previous reports
496 (Liu et al., 2020; Thomas et al., 2016), where the resistant rice line, expressing *Xa21,* shows
497 elevation in the expression of *PR10b* while the susceptible rice line does not show elevated
498 *PR10b* expression. Essentially, we noted that blocking this early Ca^{2+} signal by Ca^{2+}-chelation
499 results in a weakened immune response in the resistant variety CR 800 (Fig. 2). Through further
500 investigation, we have observed that *Xoo*-OMV-induced nanodomain enrichment is also
501 impaired in Ca^{2+}-chelated roots (Fig. 3). As ordered PM is necessary for OMV insertion (Tran
502 et al., 2022), the disordered membrane of EGTA-treated roots show reduced *Xoo*-OMV
503 insertion (Fig. 4). Temporal analysis of the events elucidates, Ca^{2+} signalling as one of the
504 earliest event during *Xoo*-OMV perception (10 minutes after application), followed by
505 nanodomain enrichment (30 minutes after *Xoo*-OMV application) and insertion of OMVs into
506 the rice PM (after 60 minutes of incubation in *Xoo*-OMVs). Tran et al., 2022 showed that *Xcc*-
507 OMVs get inserted in the Arabidopsis PM within 10 minutes. The delay in the incorporation
508 of the *Xoo*-OMVs in rice PM (60 minutes) is probably due to the differential composition of
509 the cell walls of rice and Arabidopsis, as rice roots are more densely packed and rigid than
510 Arabidopsis roots (Vogel, 2008).

511 Based on these observations, we hypothesized that Ca^{2+} signalling led to aggregation of
512 specific proteins in the rice PM, which shapes the response of rice towards *Xoo*-OMVs. To
513 verify our hypothesis, we performed quantitative proteomics analysis of CR 800 root PM after
514 *Xoo*-OMV application, both in the presence and absence of Ca^{2+}-chelator (EGTA). We
515 observed that several defence response-related proteins were significantly upregulated in CR
516 800 OMV-treated roots but not in EGTA-OMV-treated roots, validating the compromised
517 immune response displayed on Ca^{2+}-chelation. Several sterol and lipid biosynthesis pathway-
518 related proteins were also more abundant after *Xoo*-OMV application, which leads to a highly
519 ordered PM (Fig. 5, Table 1). Contrastingly, in a Ca^{2+}-deprived condition, these proteins were
520 not significantly upregulated, which might lead to a disordered membrane, as manifested in
521 Di-4-staining assay (Fig. 3). Similarly, membrane organisation and nanodomain-associated
522 proteins like remorins, syntaxins, annexin, tetraspanins, etc, which aid in vesicle fusion and

523 docking, are highly abundant in OMV-treated roots, but not in roots treated with EGTA-OMV-
524 treated roots (Fig. 5, Table 1).

525 Taken together, our outcomes reveal that *Xoo* releases OMVs that comprise abundant MAMPs
526 and virulence-associated proteins. These MAMP-loaded *Xoo*-OMVs are sensed by the plant,
527 via a Ca^{2+} signal generation. The Ca^{2+} signal enables the organization of a nanodomain-
528 enriched membrane possibly by upregulating the sterol biosynthesis pathway and leads to the
529 aggregation of specialized defence proteins in the rice PM. These proteins transduce the signal
530 downstream and generate an immune response against the pathogen. Remorins, annexins,
531 ankyrin repeat-containing proteins, and SNARE proteins like syntaxins, aggregate in the
532 membrane, which might aid in the insertion of *Xoo*-OMVs into the rice PM. Such nanodomain
533 congregation is necessary to prepare the cell for a subsequent response to combat the
534 pathogenic challenge by recruiting the defence-related proteins into signalling hubs. In a Ca^{2+}-
535 deprived condition, these proteins are not efficiently assembled in the PM, resulting in a
536 perturbed recognition of *Xoo*-OMVs by the plant and a disrupted immune response. Although,
537 Khitish, the susceptible variety, could perceive the *Xoo*-OMVs through Ca^{2+} signal generation,
538 nanodomain enrichment and insertion of *Xoo*-OMVs into the rice PM, it failed to evoke any
539 immune response due to the absence of R genes and the associated repertoire of proteins
540 (Figure 6).

541 Remarkably, specific nanodomains are organized with appropriate proteins and function in a
542 signal-specific manner (Bücherl et al., 2017). However, the mechanism of such signal-specific
543 nanodomain assembly is still elusive. We propose that the precise and spatiotemporally unique
544 Ca^{2+} signals exhibited in response to different biotic and abiotic stimuli can stipulate such a
545 signal-specific nanodomain formation. Further research is required to uncover the molecular
546 mechanism of Ca^{2+}-mediated nanodomain configuration to understand the recruitment of the
547 various signalling components at the plant plasma membrane.

548 **Acknowledgments**

549 This work was funded by the SRG/2022/002293 grant from the Department of Science and
550 Technology Government of India. We thank Dr. H. K. Patel from CSIR-CCMB for providing
551 us with the *Xoo* strains that have been used in the study. We are thankful to the Rice Research
552 Station, Chinsurah, West Bengal, for providing us with the seeds of Khitish and CR 800. We
553 acknowledge the Central Instrumentation Facility (CIF) of CSIR-Indian Institute of Chemical

554 Biology (CSIR-IICB). We are thankful to DBT-ILS for the TEM and ESI-MS/MS experiments.
555 We Acknowledge Mr. Sandip Barman for critically reading the manuscript for editing.

556 **Competing interests:**

557 The authors declare that they have no competing interests.

558 **Author contributions:**

559 SB conceptualized the project and arranged the funding. IM and SB designed the experiments.
560 IM and HD performed the experiments. IM and SB analysed the data. IM and SB wrote the
561 manuscript.

562 **Data availability:**

563 All the data discussed in the manuscript are included as supplementary information. All of the
564 proteins identified from the *Xoo*-OMV-associated proteome and CR 800 PM-associated
565 proteome analysis are listed in the supplementary tables, Table 1 and Table 2, respectively.
566 Raw files of proteomic analysis are available on request.

567 **References**

568 Ali, R., Ma, W., Lemtiri-Chlieh, F., Tsaltas, D., Leng, Q., Von Bodman, S., Berkowitz, G.A., 2007. Death
569 Don't Have No Mercy and Neither Does Calcium: Arabidopsis CYCLIC NUCLEOTIDE GATED
570 CHANNEL2 and Innate Immunity. Plant Cell 19, 1081–1095. https://doi.org/10.1105/tpc.106.045096

571 Bahar, O., Mordukhovich, G., Luu, D.D., Schwessinger, B., Daudi, A., Jehle, A.K., Felix, G., Ronald, P.C.,
572 2016. Bacterial Outer Membrane Vesicles Induce Plant Immune Responses. Mol. Plant-Microbe
573 Interactions® 29, 374–384. https://doi.org/10.1094/MPMI-12-15-0270-R

574 Bao, Y.-M., Sun, S.-J., Li, M., Li, L., Cao, W.-L., Luo, J., Tang, H.-J., Huang, J., Wang, Z. F., Wang, J.-F.,
575 Zhang, H.-S., 2012. Overexpression of the Qc-SNARE gene OsSYP71 enhances tolerance to oxidative
576 stress and resistance to rice blast in rice (Oryza sativa L.). Gene 504, 238–244.
577 https://doi.org/10.1016/j.gene.2012.05.011

578 Behera, S., Wang, N., Zhang, C., Schmitz-Thom, I., Strohkamp, S., Schültke, S., Hashimoto, K., Xiong, L.,
579 Kudla, J., 2015. Analyses of Ca2+ dynamics using a ubiquitin-10 promoter-driven Yellow Cameleon 3.6
580 indicator reveal reliable transgene expression and differences in cytoplasmic Ca2+ responses in Arabidopsis
581 and rice (Oryza sativa) roots. New Phytol. 206, 751–760. https://doi.org/10.1111/nph.13250

582 Bücherl, C.A., Jarsch, I.K., Schudoma, C., Segonzac, C., Mbengue, M., Robatzek, S., MacLean, D., Ott, T.,
583 Zipfel, C., 2017. Plant immune and growth receptors share common signalling components but localise to
584 distinct plasma membrane nanodomains. eLife 6, e25114. https://doi.org/10.7554/eLife.25114

585 Bundó, M., Coca, M., 2017. Calcium-dependent protein kinase OsCPK10 mediates both drought tolerance
586 and blast disease resistance in rice plants. J. Exp. Bot. 68, 2963–2975. https://doi.org/10.1093/jxb/erx145

587 Cao, J., Yang, C., Li, L., Jiang, L., Wu, Y., Wu, C., Bu, Q., Xia, G., Liu, X., Luo, Y., Liu, J., 2016. Rice
588 Plasma Membrane Proteomics Reveals Magnaporthe oryzae Promotes Susceptibility by Sequential
589 Activation of Host Hormone Signalling Pathways. Mol. Plant-Microbe Interactions® 29, 902–913.
590 https://doi.org/10.1094/MPMI-08-16-0165-R

591 Cao, W.-L., Yu, Y., Li, M.-Y., Luo, J., Wang, R.-S., Tang, H.-J., Huang, J., Wang, J.-F., Zhang, H.-S., Bao,
592 Y.-M., 2019. OsSYP121 Accumulates at Fungal Penetration Sites and Mediates Host Resistance to Rice
593 Blast. Plant Physiol. 179, 1330–1342. https://doi.org/10.1104/pp.18.01013

594 Cao, X.-Q., Jiang, Z.-H., Yi, Y.-Y., Yang, Y., Ke, L.-P., Pei, Z.-M., Zhu, S., 2017. Biotic and Abiotic
595 Stresses Activate Different Ca2+ Permeable Channels in Arabidopsis. Front. Plant Sci. 8.
596 https://doi.org/10.3389/fpls.2017.00083

597 Chalupowicz, L., Mordukhovich, G., Assoline, N., Katsir, L., Sela, N., Bahar, O., 2023. Bacterial outer
598 membrane vesicles induce a transcriptional shift in arabidopsis towards immune system activation leading
599 to suppression of pathogen growth in planta. J. Extracell. Vesicles 12, 12285.
600 https://doi.org/10.1002/jev2.12285

601 Chatterjee, S., Sankaranarayanan, R., Sonti, R.V., 2003. PhyA, a Secreted Protein of Xanthomonas oryzae
602 pv. oryzae, Is Required for Optimum Virulence and Growth on Phytic Acid as a Sole Phosphate Source.
603 Mol. Plant-Microbe Interactions® 16, 973–982. https://doi.org/10.1094/MPMI.2003.16.11.973

604 Chen, F., Yuan, Y., Li, Q., He, Z., 2007. Proteomic analysis of rice plasma membrane reveals proteins
605 involved in early defence response to bacterial blight. PROTEOMICS 7, 1529–1539.
606 https://doi.org/10.1002/pmic.200500765

607 Chen, X., Zuo, S., Schwessinger, B., Chern, M., Canlas, P.E., Ruan, D., Zhou, X., Wang, J., Daudi, A.,
608 Petzold, C.J., Heazlewood, J.L., Ronald, P.C., 2014. An XA21-associated kinase (OsSERK2) regulates
609 immunity mediated by the XA21 and XA3 immune receptors. Mol. Plant 7, 874–892.
610 https://doi.org/10.1093/mp/ssu003

611 Chowdhury, C., Jagannadham, M.V., 2013. Virulence factors are released in association with outer
612 membrane vesicles of Pseudomonas syringae pv. tomato T1 during normal growth. Biochim. Biophys. Acta
613 BBA - Proteins Proteomics 1834, 231–239. https://doi.org/10.1016/j.bbapap.2012.09.015

614 Das, A., Rangaraj, N., Sonti, R.V., 2009. Multiple Adhesin-Like Functions of Xanthomonas oryzae pv.
615 oryzae Are Involved in Promoting Leaf Attachment, Entry, and Virulence on Rice. Mol. Plant-Microbe
616 Interactions® 22, 73–85. https://doi.org/10.1094/MPMI-22-1-0073

617 Feitosa-Junior, O.R., Stefanello, E., Zaini, P.A., Nascimento, R., Pierry, P.M., Dandekar, A.M., Lindow,
618 S.E., Da Silva, A.M., 2019. Proteomic and Metabolomic Analyses of Xylella fastidiosa OMV-Enriched
619 Fractions Reveal Association with Virulence Factors and Signaling Molecules of the DSF Family.
620 Phytopathology 109, 1344–1353. https://doi.org/10.1094/PHYTO-03-19-0083-R

621 Fujiwara, M., Hamada, S., Hiratsuka, M., Fukao, Y., Kawasaki, T., Shimamoto, K., 2009. Proteome
622 Analysis of Detergent-Resistant Membranes (DRMs) Associated with OsRac1-Mediated Innate Immunity
623 in Rice. Plant Cell Physiol. 50, 1191–1200. https://doi.org/10.1093/pcp/pcp077

624 Grant, M., Brown, I., Adams, S., Knight, M., Ainslie, A., Mansfield, J., 2000. The RPM1 plant disease
625 resistance gene facilitates a rapid and sustained increase in cytosolic calcium that is necessary for the
626 oxidative burst and hypersensitive cell death. Plant J. 23, 441–450. https://doi.org/10.1046/j.1365-
627 313x.2000.00804.x

628 Gronnier, J., Crowet, J.-M., Habenstein, B., Nasir, M.N., Bayle, V., Hosy, E., Platre, M.P., Gouguet, P.,
629 Raffaele, S., Martinez, D., Grelard, A., Loquet, A., Simon-Plas, F., Gerbeau-Pissot, P., Der, C., Bayer,
630 E.M., Jaillais, Y., Deleu, M., Germain, V., Lins, L., Mongrand, S., 2017. Structural basis for plant plasma
631 membrane protein dynamics and organization into functional nanodomains. eLife 6, e26404.
632 https://doi.org/10.7554/eLife.26404

633 Gui, J., Zheng, S., Liu, C., Shen, J., Li, J., Li, L., 2016. OsREM4.1 Interacts with OsSERK1 to Coordinate
634 the Interlinking between Abscisic Acid and Brassinosteroid Signaling in Rice. Dev. Cell 38, 201–213.
635 https://doi.org/10.1016/j.devcel.2016.06.011

636 Guo, X., Cheng, Z., Wang, Jiulin, Tian, Y., Liu, S., Jiang, L., Wu, C., Wang, E., Zhou, J.-M., Wang, Y.-F.,
637 Wang, H., Wan, J., 2019. A cyclic nucleotide-gated channel mediates cytoplasmic calcium elevation and
638 disease resistance in rice. Cell Res. 29, 820–831. https://doi.org/10.1038/s41422-019-0219-7

639 Huang, Y., Zhu, F., Koh, J., Stanton, D., Chen, S., Wang, N., 2022. Proteomic and bioinformatic analyses
640 of proteins in the outer membrane and extracellular compartments and outer membrane vesicles of
641 Candidatus Liberibacter species. Front. Microbiol. 13, 977710. https://doi.org/10.3389/fmicb.2022.977710

642 Jaillais, Y., Ott, T., 2020. The Nanoscale Organization of the Plasma Membrane and Its Importance in
643 Signalling: A Proteolipid Perspective. Plant Physiol. 182, 1682–1696.
644 https://doi.org/10.1104/pp.19.01349

645 Jang, K.-S., Sweredoski, M.J., Graham, R.L.J., Hess, S., Clemons, W.M., 2014. Comprehensive proteomic
646 profiling of outer membrane vesicles from Campylobacter jejuni. J. Proteomics 98, 90–98.
647 https://doi.org/10.1016/j.jprot.2013.12.014

648 Kaparakis-Liaskos, M., Ferrero, R.L., 2015. Immune modulation by bacterial outer membrane vesicles. Nat.
649 Rev. Immunol. 15, 375–387. https://doi.org/10.1038/nri3837

650 Keinath, N.F., Waadt, R., Brugman, R., Schroeder, J.I., Grossmann, G., Schumacher, K., Krebs, M., 2015.
651 Live Cell Imaging with R-GECO1 Sheds Light on flg22- and Chitin-Induced Transient [Ca 2+] cyt Patterns
652 in Arabidopsis. Mol. Plant 8, 1188–1200. https://doi.org/10.1016/j.molp.2015.05.006

653 Kim, J., Jung, J.H., Lee, S.B., Go, Y.S., Kim, H.J., Cahoon, R., Markham, J.E., Cahoon, E.B., Suh, M.C.,
654 2013. Arabidopsis 3-ketoacyl-coenzyme a synthase9 is involved in the synthesis of tetracosanoic acids as
655 precursors of cuticular waxes, suberins, sphingolipids, and phospholipids. Plant Physiol. 162, 567–580.
656 https://doi.org/10.1104/pp.112.210450

657 Komatsu, S., 2008. Plasma membrane proteome in Arabidopsis and rice. PROTEOMICS 8, 4137–4145.
658 https://doi.org/10.1002/pmic.200800088

659 Kulp, A., Kuehn, M.J., 2010. Biological Functions and Biogenesis of Secreted Bacterial Outer Membrane
660 Vesicles. Annu. Rev. Microbiol. 64, 163–184. https://doi.org/10.1146/annurev.micro.091208.073413

661 Lappann, M., Otto, A., Becher, D., Vogel, U., 2013. Comparative

662 Li, H., Zhou, S.-Y., Zhao, W.-S., Su, S.-C., Peng, Y.-L., 2009. A novel wall-associated receptor-like protein
663 kinase gene, OsWAK1, plays important roles in rice blast disease resistance. Plant Mol. Biol. 69, 337–346.
664 https://doi.org/10.1007/s11103-008-9430-5

665 Liu, F., Zhang, W., Schwessinger, B., Wei, T., Ruan, D., Ronald, P., 2020. The Rice Xa3 Gene Confers
666 Resistance to Xanthomonas oryzae pv. oryzae in the Model Rice Kitaake Genetic Background. Front. Plant
667 Sci. 11, 49. https://doi.org/10.3389/fpls.2020.00049

668 Liu, Z., Qiu, J., Shen, Z., Wang, C., Jiang, N., Shi, H., Kou, Y., 2023. The E3 ubiquitin ligase OsRGLG5
669 targeted by the Magnaporthe oryzae effector AvrPi9 confers basal resistance against rice blast. Plant
670 Commun. 4, 100626. https://doi.org/10.1016/j.xplc.2023.100626

671 Malukani, K.K., Ranjan, A., Hota, S.J., Patel, H.K., Sonti, R.V., 2020. Dual Activities of Receptor-Like
672 Kinase OsWAKL21.2 Induce Immune Responses. Plant Physiol. 183, 1345–1363.
673 https://doi.org/10.1104/pp.19.01579

674 Maphosa, S., Moleleki, L.N., 2021. Isolation and Characterization of Outer Membrane Vesicles of
675 Pectobacterium brasiliense 1692. Microorganisms 9, 1918. https://doi.org/10.3390/microorganisms9091918

676 McBroom, A.J., Kuehn, M.J., 2007. Release of outer membrane vesicles by Gram-negative bacteria is a
677 novel envelope stress response. Mol. Microbiol. 63, 545–558. https://doi.org/10.1111/j.1365-
678 2958.2006.05522.x

679 McMillan, H.M., Kuehn, M.J., 2021. The extracellular vesicle generation paradox: a bacterial point of view.
680 EMBO J. 40, e108174. https://doi.org/10.15252/embj.2021108174

681 McMillan, H.M., Kuehn, M.J., 2023. Proteomic Profiling Reveals Distinct Bacterial Extracellular Vesicle
682 Subpopulations with Possibly Unique Functionality. Appl. Environ. Microbiol. 89, e01686-22.
683 https://doi.org/10.1128/aem.01686-22

684 McMillan, H.M., Zebell, S.G., Ristaino, J.B., Dong, X., Kuehn, M.J., 2021. Protective plant immune
685 responses are elicited by bacterial outer membrane vesicles. Cell Rep. 34, 108645.
686 https://doi.org/10.1016/j.celrep.2020.108645

687 Mendes, J.S., Santiago, A.S., Toledo, M.A.S., Horta, M.A.C., De Souza, A.A., Tasic, L., De Souza, A.P.,
688 2016. In vitro Determination of Extracellular Proteins from Xylella fastidiosa. Front. Microbiol. 7.
689 https://doi.org/10.3389/fmicb.2016.02090

690 Mohapatra, S., Barik, S.R., Dash, P.K., Lenka, D., Pradhan, K.C., Raj K. R, R., Mohanty, S.P., Mohanty,
691 M.R., Sahoo, A., Jena, B.K., Panda, A.K., Panigrahi, D., Dash, S.K., Meher, J., Sahoo, C.R., Mukherjee,
692 A.K., Das, L., Behera, L., Pradhan, S.K., 2023. Molecular Breeding for Incorporation of Submergence
693 Tolerance and Durable Bacterial Blight Resistance into the Popular Rice Variety 'Ranidhan.' Biomolecules
694 13, 198. https://doi.org/10.3390/biom13020198

695 Mordukhovich, G., Bahar, O., 2017. Isolation of Outer Membrane Vesicles from Phytopathogenic
696 Xanthomonas campestris pv. campestris. BIO-Protoc. 7. https://doi.org/10.21769/BioProtoc.2160

697 Mou, B., Zhao, G., Wang, J., Wang, S., He, F., Ning, Y., Li, D., Zheng, X., Cui, F., Xue, F., Zhang, S., Sun,
698 W., 2024. The OsCPK17-OsPUB12-OsRLCK176 module regulates immune homeostasis in rice. Plant Cell
699 36, 987–1006. https://doi.org/10.1093/plcell/koad265

700 Nagano, M., Ishikawa, T., Fujiwara, M., Fukao, Y., Kawano, Y., Kawai-Yamada, M., Shimamoto, K.,
701 2016. Plasma Membrane Microdomains Are Essential for Rac1-RbohB/H-Mediated Immunity in Rice.
702 Plant Cell 28, 1966–1983. https://doi.org/10.1105/tpc.16.00201

703 Naqvi, S.A.H., 2019. Bacterial Leaf Blight of Rice: An Overview of Epidemiology and Management with
704 Special Reference to-Indian-Sub-Continent. Pak. J. Agric. Res. 32.
705 https://doi.org/10.17582/journal.pjar/2019/32.2.359.380

706 Niño-Liu, D.O., Ronald, P.C., Bogdanove, A.J., 2006. Xanthomonas oryzae pathovars: model pathogens of
707 a model crop. Mol. Plant Pathol. 7, 303–324. https://doi.org/10.1111/j.1364-3703.2006.00344.x

708 Ott, T., 2017. Membrane nanodomains and microdomains in plant–microbe interactions. Curr. Opin. Plant
709 Biol. 40, 82–88. https://doi.org/10.1016/j.pbi.2017.08.008

710 Owen, D.M., Rentero, C., Magenau, A., Abu-Siniyeh, A., Gaus, K., 2012. Quantitative imaging of
711 membrane lipid order in cells and organisms. Nat. Protoc. 7, 24–35. https://doi.org/10.1038/nprot.2011.419

712 Paniagua, C., Bilkova, A., Jackson, P., Dabravolski, S., Riber, W., Didi, V., Houser, J., Gigli-Bisceglia, N.,
713 Wimmerova, M., Budínská, E., Hamann, T., Hejatko, J., 2017. Dirigent proteins in plants: modulating cell
714 wall metabolism during abiotic and biotic stress exposure. J. Exp. Bot. 68, 3287–3301.
715 https://doi.org/10.1093/jxb/erx141

716 Perraki, A., Gronnier, J., Gouguet, P., Boudsocq, M., Deroubaix, A.-F., Simon, V., German-Retana, S.,
717 Legrand, A., Habenstein, B., Zipfel, C., Bayer, E., Mongrand, S., Germain, V., 2018. REM1.3's phospho-
718 status defines its plasma membrane nanodomain organization and activity in restricting PVX cell-to-cell
719 movement. PLOS Pathog. 14, e1007378. https://doi.org/10.1371/journal.ppat.1007378

720 Rajagopal, L., Sundari, C.S., Balasubramanian, D., Sonti, R.V., 1997. The bacterial pigment
721 xanthomonadin offers protection against photodamage. FEBS Lett. 415, 125–128.
722 https://doi.org/10.1016/S0014-5793(97)01109-5

723 Ranf, S., Eschen-Lippold, L., Fröhlich, K., Westphal, L., Scheel, D., Lee, J., 2014. Microbe-associated
724 molecular pattern-induced calcium signalling requires the receptor-like cytoplasmic kinases, PBL1 and
725 BIK1. BMC Plant Biol. 14, 374. https://doi.org/10.1186/s12870-014-0374-4

726 Ranf, S., Gisch, N., Schäffer, M., Illig, T., Westphal, L., Knirel, Y.A., Sánchez-Carballo, P.M., Zähringer,
727 U., Hückelhoven, R., Lee, J., Scheel, D., 2015. A lectin S-domain receptor kinase mediates
728 lipopolysaccharide sensing in Arabidopsis thaliana. Nat. Immunol. 16, 426–433.
729 https://doi.org/10.1038/ni.3124

730 Sartorio, M.G., Pardue, E.J., Feldman, M.F., Haurat, M.F., 2021. Bacterial Outer Membrane Vesicles: From
731 Discovery to Applications. Annu. Rev. Microbiol. 75, 609–630. https://doi.org/10.1146/annurev-micro-
732 052821-031444

733 Schaar, V., De Vries, S.P.W., Perez Vidakovics, M.L.A., Bootsma, H.J., Larsson, L., Hermans, P.W.M.,
734 Bjartell, A., Mörgelin, M., Riesbeck, K., 2011. Multicomponent Moraxella catarrhalis outer membrane
735 vesicles induce an inflammatory response and are internalized by human epithelial cells: Characterization
736 of M. catarrhalis OMVs. Cell. Microbiol. 13, 432–449. https://doi.org/10.1111/j.1462-5822.2010.01546.x

737 Schwechheimer, C., Kuehn, M.J., 2015. Outer-membrane vesicles from Gram-negative bacteria: biogenesis
738 and functions. Nat. Rev. Microbiol. 13, 605–619. https://doi.org/10.1038/nrmicro3525

739 Sidhu, V.K., Vorhölter, F.-J., Niehaus, K., Watt, S.A., 2008. Analysis of outer membrane vesicle associated
740 proteins isolated from the plant pathogenic bacterium Xanthomonas campestris pv. campestris. BMC
741 Microbiol. 8, 87. https://doi.org/10.1186/1471-2180-8-87

742 Smokvarska, M., Francis, C., Platre, M.P., Fiche, J.-B., Alcon, C., Dumont, X., Nacry, P., Bayle, V.,
743 Nollmann, M., Maurel, C., Jaillais, Y., Martiniere, A., 2020. A Plasma Membrane Nanodomain Ensures
744 Signal Specificity during Osmotic Signalling in Plants. Curr. Biol. 30, 4654-4664.e4.
745 https://doi.org/10.1016/j.cub.2020.09.013

746 Subramoni, S., Pandey, A., Vishnu Priya, M.R., Patel, H.K., Sonti, R.V., 2012. The ColRS system of
747 Xanthomonas oryzae pv. oryzae is required for virulence and growth in iron-limiting conditions. Mol. Plant
748 Pathol. 13, 690–703. https://doi.org/10.1111/j.1364-3703.2011.00777.x

749 Thomas, N.C., Schwessinger, B., Liu, F., Chen, H., Wei, T., Nguyen, Y.P., Shaker, I.W.F., Ronald, P.C.,
750 2016. XA21-specific induction of stress-related genes following Xanthomonas infection of detached rice
751 leaves. PeerJ 4, e2446. https://doi.org/10.7717/peerj.2446

752 Tian, W., Hou, C., Ren, Z., Wang, C., Zhao, F., Dahlbeck, D., Hu, S., Zhang, L., Niu, Q., Li, L.,
753 Staskawicz, B.J., Luan, S., 2019. A calmodulin-gated calcium channel links pathogen patterns to plant
754 immunity. Nature 572, 131–135. https://doi.org/10.1038/s41586-019-1413-y

755 Tran, T.M., Chng, C.-P., Pu, X., Ma, Z., Han, X., Liu, X., Yang, L., Huang, C., Miao, Y., 2022.
756 Potentiation of plant defence by bacterial outer membrane vesicles is mediated by membrane nanodomains.
757 Plant Cell 34, 395–417. https://doi.org/10.1093/plcell/koab276

758 Uemura, M., Joseph, R.A., Steponkus, P.L., 1995. Cold Acclimation of Arabidopsis thaliana (Effect on
759 Plasma Membrane Lipid Composition and Freeze-Induced Lesions). Plant Physiol. 109, 15–30.
760 https://doi.org/10.1104/pp.109.1.15

761 Vogel, J., 2008. Unique aspects of the grass cell wall. Curr. Opin. Plant Biol. 11, 301–307.
762 https://doi.org/10.1016/j.pbi.2008.03.002

763 Wang, Jiachang, Liu, X., Zhang, A., Ren, Y., Wu, F., Wang, G., Xu, Y., Lei, C., Zhu, S., Pan, T., Wang,
764 Yongfei, Zhang, H., Wang, F., Tan, Y.-Q., Wang, Yupeng, Jin, X., Luo, S., Zhou, C., Zhang, Xiao, Liu, J.,
765 Wang, S., Meng, L., Wang, Yihua, Chen, X., Lin, Q., Zhang, Xin,

766 Yang, C., Liu, R., Pang, J., Ren, B., Zhou, H., Wang, G., Wang, E., Liu, J., 2021. Poaceae-specific cell
767 wall-derived oligosaccharides activate plant immunity via OsCERK1 during Magnaporthe oryzae infection
768 in rice. Nat. Commun. 12, 2178. https://doi.org/10.1038/s41467-021-22456-x

769 Yang, Z., Xing, J., Wang, L., Liu, Y., Qu, J., Tan, Y., Fu, X., Lin, Q., Deng, H., Yu, F., 2020. Mutations of
770 two FERONIA-like receptor genes enhance rice blast resistance without growth penalty. J. Exp. Bot. 71,
771 2112–2126. https://doi.org/10.1093/jxb/erz541

772 Young, S.A., Wang, X., Leach, J.E., 1996. Changes in the Plasma Membrane Distribution of Rice
773 Phospholipase D during Resistant Interactions with Xanthomonas oryzae pv oryzae. Plant Cell 1079–1090.
774 https://doi.org/10.1105/tpc.8.6.1079

775 Zhang, H., Chen, C., Li, L., Tan, X., Wei, Z., Li, Y., Li, J., Yan, F., Chen, J., Sun, Z., 2021. A rice LRR
776 receptor-like protein associates with its adaptor kinase OsSOBIR1 to mediate plant immunity against viral
777 infection. Plant Biotechnol. J. 19, 2319–2332. https://doi.org/10.1111/pbi.13663

778

779 **Figure legends:**

780 **Fig. 1.** Characterization of *Xoo*-OMVs and identification of their protein content. a, AFM
781 images showing the release of BXO43 OMVs into their surroundings by blebbing. b, AFM
782 image of spherical *Xoo*-OMVs. c, the hydrodynamic size range of the *Xoo*-OMVs (125.8 +/-
783 1.6 nm) exhibited by NTA. d, TEM image of *Xoo*-OMVs including smaller vesicles (10-60nm),
784 indicated by the yellow arrow, and bigger vesicles (100-150nm), indicated by the white arrow.
785 e, Subcellular localization of 423 proteins identified by proteomic analysis of *Xoo*-OMVs (n=4)
786 are designated using String Database. f and g, predicted biological, and molecular functions of
787 the proteins, appointed using String Database are represented in lollipop charts, with strength
788 ($\log_{10}$(Expected/Observed)) in the x-axis.

789 **Fig. 2.** *Xoo*-OMVs induce cellular Ca^{2+} elevation in rice and Arabidopsis roots. a and b, 7-day-old
790 Khitish and CR 800 roots, respectively, stained with Calcium Green1, AM, showing an increase in
791 cellular Ca^{2+} when treated with *Xoo*-OMVs. No Ca^{2+} elevation was observed with solvent treatment,
792 scale bar=125 μm. c and d, the relative fluorescence of the Khitish and CR 800 roots after treatment
793 with *Xoo*-OMVs and solvent control were plotted as a histogram at intervals of 5 minutes using
794 GraphPad Prism software (n=6). Student's t-test was done to deduce the statistical difference between
795 the fluorescence of control and *Xoo*-OMV-treated roots at each time point, n=6. e, 4-day-old
796 Arabidopsis Col-0 roots, expressing Ca^{2+} indicator protein RGECO1 treated with *Xoo*-OMVs. showing
797 an increase in fluorescence, indicating a Ca^{2+} spike after treatment with *Xoo*-OMVs, scale bar=50 μm.
798 f, selection of ROIs, namely, the meristematic region (ROI1), the distal elongation region (ROI2), and
799 the central elongation region (ROI3). g, the average line curve (n=5) showing the Ca^{2+} signal induced
800 by *Xoo*-OMVs in different ROIs of the Arabidopsis roots with respect to time. The black arrow indicates
801 the time of application of *Xoo*-OMVs. h, the relative expression of the *PR10b* gene after incubation in
802 *Xoo*-OMVs for 1 hour (in the presence and absence of Ca^{2+}-chelator) in CR 800 and Khitish roots, (n=3
803 independent replicates). The statistical differences have been calculated through one-way ANOVA
804 using GraphPad Prism software (ns, not significant, *P≤0.05; **P≤0.01, ***P≤0.001, ****P≤0.0001).

805 **Fig. 3** Ca^{2+} and sterol-dependent lipid order increase in rice PM after incubation in *Xoo*-OMVs. a, 7-
806 day-old Khitish and CR 800 roots incubated with *Xoo*-OMVs for 30 min and stained with Di-4-
807 ANEPPDHQ showing an increase in the lipid order of rice PM (n≥6 seedlings). 30-minute pre-treatment
808 with BAPTA-AM (25 μM) or EGTA (2 mM) inhibits lipid order increase. b, GP values (-1 to +1) have
809 been calculated using ImageJ software and plotted in a Box-plot using GraphPad Prism software, the
810 corresponding statistical significance have been calculated through one-way ANOVA (p≤0.05), c, leaf
811 protoplasts isolated from Khitish and CR 800 showing lipid order rise after incubation with *Xoo*-OMVs.
812 BAPTA-AM (25 μM) or MβCD (2 mM) pre-treated protoplasts not showing significant rise in lipid
813 order even after *Xoo*-OMV exposure. d, GP values of the protoplast membrane of Khitish and CR 800,
814 represented in a box plot. The statistical significance has been calculated by one-way ANOVA using
815 GraphPad Prism software (ns, not significant, *P≤0.05; **P≤0.01, ***P≤0.001, ****P≤0.0001).

816 **Fig. 4.** *Xoo*-OMVs get inserted into rice PM. a, 7-day-old Khitish and CR 800 roots showing a
817 significant decrease in *Xoo*-OMV insertion on Ca^{2+}-chelation and sterol-depletion with BAPTA-AM
818 (25 μM) and MβCD (2 mM), respectively (n≥7 seedlings), scale bar=20 μm. b, histogram showing the

statistical difference between the relative fluorescence units of each sample, calculated using one-way ANOVA by GraphPad Prism. c, FM4-64 stained *Xoo*-OMVs inserted into the PM of leaf protoplasts with and without pre-treatment with BAPTA-AM (25 μM). d, GraphPad Prism was used to create the histograms and analyse the statistical difference between the protoplast samples through one-way ANOVA, (ns, not significant, *P≤0.05; **P≤0.01, ***P≤0.001, ****P≤0.0001).

Fig. 5. Analysis of the CR 800 PM proteome remodelling after *Xoo*-OMV treatment in native and Ca^{2+}-deprived condition. a, Functional annotations of the 233 proteins upregulated (1.5≥Fold-change, p≤0.05) in CR 800 PM after *Xoo*-OMV treatment in normal condition, but not in a Ca^{2+}-chelated condition. Enrichment is represented as a lollipop chart created using String Database with strength (log_{10}(Expected/Observed)) in the x-axis. b, Heatmap displays the abundance of key proteins involved in important pathways as observed after different treatments, Control (sterile water-1hr), EGTA-OMV (30 min pre-treatment with EGTA (2mM); *Xoo*-OMV-1hr), and OMV (*Xoo*-OMV-1hr), (n=3).

Fig. 6. Ca^{2+}-dependent perception of *Xoo*-OMVs by rice via nanodomain-mediated PM proteome reorganization. *Xoo*-OMVs are associated with MAMPs and virulence-associated proteins. Through these MAMPs, the rice cell recognizes the *Xoo*-OMVs by evoking a Ca^{2+} signal. This leads to nanodomain enrichment in the rice PM and shifts the PM proteome towards the defence response pathway. It also enables insertion of *Xoo*-OMVs into the rice PM. Both Khitish and CR 800 perceive the *Xoo*-OMVs similarly, but, the resistant variety CR 800, expressing R genes (*Xa21*, *xa13, xa5*) mounts an immune response against the pathogen, while Khitish the susceptible variety without any R gene cannot evoke any immune response. If the early Ca^{2+} signal is blocked, *Xoo*-OMV perception and following immune response are impaired in CR 800.

Supporting Information

The following Supporting Information is available for this article:

Fig. S1 Temporal nanodomain enrichment in rice roots after exposure to *Xoo*-OMVs in Ca^{2+}-chelated condition.

Fig. S2 Insertion of *Xoo*-OMVs into the PM of rice with respect to time.

Fig. S3 Overview of CR 800 PM proteome.

Fig. S4 Functional annotation of upregulated proteins.

Table S1 All the proteins identified in the Xoo-OMVs.

Table S2 All the proteins identified in the CR 800 PM.

Video S1 Ca^{2+} signal in Arabidopsis Col-0-RGECO1 root after Xoo-OMV application.